https://doi.org/10.5194/wes-2025-155
Preprint. Discussion started: 20 October 2025

eawe european academy of wind energy
Open Access WIND ENERGY SCIENCE DISCUSSIONS

Comparing atmospheric boundary layer heights from vertical profiling scanning lidars to ERA5 and WRF

Cristina Mulet-Benzo[1,2], Andrew Black[3], and Julia Gottschall[1,2]

[1]Fraunhofer Institute for Wind Energy Systems IWES, Bremen, Germany
[2]University of Bremen, Germany
[3]Vaisala France, Saclay, France

Correspondence: Cristina Mulet-Benzo (cristina.mulet-benzo@fraunhofer.iwes.de)

Abstract.

The expansion and creation of new wind farms in recent years brings up challenges to manage both inter- and intra- wind farm wake effects. Wake blockage impact heavily relies on atmospheric conditions for determining how long and how intense the wake propagation is. One of these key atmospheric parameters is the height of the atmospheric boundary layer (ABL), which determines the height of the atmosphere most impacted by surface layer wind speed and temperature regimes. Generally lower ABL is united with more stable conditions, and thus greater the wake propagation. Offshore wind farms experience more frequent stable conditions compared to onshore farms, thus boundary layer conditions must be well parameterized to accurately model wake blockage effects. Scanning lidars present a viable solution for boundary layer height determination. In this study, their measurements are compared against ERA5 and WRF ABL model outputs. The lidar acts as a reference for boundary layer conditions, categorizing the ABL for both the mixing (convectively driven) and residual (stably driven) layer heights. Two campaigns, both using WindCube Scan devices, were assessed: one located completely offshore and another on a coastline. The results demonstrate an overestimation of the boundary layer height from both ERA5 and WRF from the offshore site of around 400m. The coastal site yielded mixed results when comparing the ABL model height to the mixing and residual layer heights derived from the lidar, with a model overestimation compared to the mixing height of 300m and for the residual height of 750m. A sensitivity study demonstrates the bias of both models correlates to the ABL diurnal cycle and to temperature flux misrepresentation in the model.

1 Introduction

Offshore wind development has made incredible advancements in the last decade, highlighting the need for well-informed resource assessments as these wind farms expand. As wind farms grow larger and more densely concentrated, understanding the atmospheric phenomena of these offshore sites elucidates the potential risks from wake clusters (Veers et al., 2022). The atmospheric boundary layer height (ABLH) defines the limit of the atmosphere where all convective activity occurs. This is where the wind speed is affected by phenomena at the surface (heat flux, friction velocity, etc.) before reaching the free atmosphere. This parameter is directly linked to atmospheric stability conditions and strongly influences momentum flux recovery in wakes (Dörenkämper et al., 2015) (Schneemann et al., 2021).

https://doi.org/10.5194/wes-2025-155
Preprint. Discussion started: 20 October 2025

eawe european academy of wind energy
Open Access WIND ENERGY SCIENCE DISCUSSIONS

Offshore conditions are mostly characterized by stably stratified conditions. These stable conditions augment wake propagation and induce turbine stress, and are normally coupled with low ABLHs, thus highlighting the importance of accurate representation (Puccioni et al., 2024) (Sood et al., 2020). Few studies exist that quantify the impact of boundary layer heights on wake propagation, such as (Sood et al., 2020). By assessing a neutral boundary layer developing against a stably stratified free atmosphere, which often occurs in offshore conditions, they found wake induced turbine loads when ABLHs were low due to greater strength of oscillations. Kalvig et al. (2014) showed that oversimplifications regarding the marine boundary layer, such as assuming a neutral boundary layer, in offshore wind applications, leads to a gross underestimation (up to 25 times lower) of lifetime turbine fatigue. Eliassen et al. (2012) and Sathe and Bierbooms (2007) also found that stable conditions give rise to greater fatigue than neutral conditions. Eliassen et al. (2012) derived an increase in damage equivalent load on rotor blades by a factor of 1.4 when considering atmospheric stability. Xu et al. (2023) concluded that, for floating offshore wind turbines, the ABLH influences power variation more than platform motions. Together, these studies show the significant impact of the ABLH and stability conditions on wake propagation, turbine lifetime, and power output, thus highlighting the need to accurately characterize this phenomenon.

Currently in meso- and micro-scale modeling the ABLH is either defined by a theoretical boundary layer scheme in numerical models, or it is set explicitly in simpler analytical models. Olsen et al. (2024) use lidar measurements to validate low level jet (LLJ) sensitivity in the Weather Research and Forecast (WRF) and the ECMWF atmospheric reanalysis of the global climate fifth generation (ERA5) models in the North and Baltic seas. They found high variability in the LLJ heights among the WRF ABL schemes, and ERA5 not capturing enough LLJ events for statistically significant comparison. Hu et al. (2010) assess three boundary layer schemes for a WRF model and compare to radiosonde data. They find the sensitivity of WRF to different ABL schemes dependent on vertical mixing strength and the resulting entrainment, meaning each scheme has its applications for particular stability conditions. Optis et al. (2014) use the ABLH as an input parameter to determine the wind profile in different stability conditions. They find the Gryning wind profile model, which incorporates the linear function of the frictional velocity and ABLH, and yields more accurate wind speeds for all stability conditions compared to the Monin-Obukhov stability theory. Munters and Meyers (2017) assess a predictive large eddy simulation (LES) model of the ABL to improve wind farm control strategies. They found an 8-21% increase in power gain but with the significant limitation of computational cost and high uncertainty in ABLH validity. Shen et al. (2024) use LES to evaluate the nocturnal stable atmospheric boundary layer, but mention limitations due to challenges in obtaining field validations. They further highlight that ABL schemes are incomplete, missing parameters that contribute to the ABLH evolution. These parameters could better define the streamwise and spanwise wind gradient scales, the Ekman length scale, the Coriolis force, surface Obukhov length, friction velocity, and various other stability parameters that rely on temperature and heat flux profile understanding.

Historically, radiosondes have been used to validate ABL model output. Radiosondes measure temperature, humidity, wind, and pressure throughout the troposphere. Guo et al. (2024) compare radiosonde data to a reanalysis dataset to bias correct ABLH data. The greatest sensitivities were attributed to land properties, near-surface meteorological conditions, terrain, lower tropospheric stability, and heat flux, with a global underestimation of the ABLH from ERA5 especially during daytime. Li et al. (2023) validate ABLHs from ERA5 to onshore radiosonde measurements in Jiangsu, China. They also find model sensitivity

https://doi.org/10.5194/wes-2025-155
Preprint. Discussion started: 20 October 2025

eawe european academy of wind energy
Open Access WIND ENERGY SCIENCE DISCUSSIONS

to the near-surface temperature, wind speed, relative humidity and lower tropospheric stability. Xi et al. (2024) evaluate the offshore ABLH from a ship campaign with radiosonde measurements in different stability conditions and compare to ERA5 outputs. They state that coarser climate models may not capture the small-scale variations of physical processes in the ABL. They find that ERA5 significantly overestimates the ABLH at low heights but underestimates the ABLH at greater heights, eliciting a smoothing tendency for ABLHs

Though radiosondes provide rich atmospheric data throughout the boundary layer, the data is limited to the launch times and locations of these devices. Doppler wind LIDAR (LIght Detection And Ranging) systems (referred to as lidar for this publication) present a viable solution to provide remote sensing measurements of the ABLH at a continuous rate, and can be easily deployed both onshore and offshore. Lidars emit laser pulses into the atmosphere and evaluate the return Doppler signal for wind speed, wind direction, aerosol concentration, and strength of the return signal. Scanning lidars provide flexible scanning patterns with a mobile scanning head and can measure the entire boundary layer with suitable atmospheric conditions. The ABLH can be derived from the lidar's measurement of vertical velocity and return signal gradients, as sharp gradient drops from these parameters represent viable indicators of residual and mixing layer heights.

ABLH validation using lidars, however, has only been a recent subject of interest. Flamant et al. (1997) represent one of the first studies to measure the marine atmospheric boundary layer from an airborne lidar. Using turbulence flux measurements from instruments of another aircraft, they validated the boundary layer height by evaluating the cumulative density distribution of the signal gradient from the airborne lidar. Bianco and Wilczak (2002) and Bianco et al. (2008) generate ABLHs using fuzzy logic method from radar signal-to-noise ratio (SNR) and vertical velocity measurements, which represent similar outputs to lidar measurements. This fuzzy logic method consists of combining the SNR and vertical velocity and variability gradients to characterize the background noise and atmospheric phenomena, then defining thresholds of when this peak occurs to define the mixed layer location. Krishnamurthy et al. (2025) used lidars to measure momentum flux using a Velocity-Azimuth Display (VAD) scan for velocity profiles. They found good correlation with surface sonic anemometers and used the lidar data to evaluate the momentum transfer in stable and unstable conditions. These continuous profiles also measured low level jet (LLJ) heights, wind farm wakes, and gravity waves. Puccioni et al. (2024) demonstrated the use of the wavelet covariance theorem (WCT) to detect the boundary layer height from lidar profiles. The WCT was used to detect sharp transitions in the SNR profiles, since above the boundary layer the density of aerosols drastically decreases. Moreira et al. (2020) use similar remote sensing technology by using ceilometer measurements to generate the ABLH. Ceilometers are a type of remote sensing instrument that measures atmospheric backscatter and aerosol concentration. They used a gradient method based on a literature review assessment and to avoid complex selection of specific parameters as required by other methods such as WCT, Ideal Fit, or Threshold Method. Abraham et al. (2024) evaluated both vertical velocity variance from scanning lidars and backscatter profiles from a ceilometer to find the ABLH impact from wind farm wakes in stable conditions. Both instruments were used to categorize stable and unstable characteristics of the ABLH. These studies provide a basis of demonstrating the practical use of scanning lidars to provide continual profiling measurements for reliable and consistent ABL measurements.

This study examines the use of offshore scanning lidar ABLH measurements to support and provide insight on model derived ABLH values. Scanning lidars for wind resource assessment are widely used and have gained trust in the wind en-

https://doi.org/10.5194/wes-2025-155
Preprint. Discussion started: 20 October 2025

ergy community for continuous reliable data for wind speed validation, wake visualization, and more (Krishnamurthy et al., 2025) (Lundquist et al., 2014) (Puccioni et al., 2024). The analysis conducted in this study consists of offshore lidar ABLH measurements compared to ERA5 and WRF model ABLH output for two offshore sites in the North sea from two separate measurement campaigns. Both scanning lidars used on the two sites are WindCube Scans with an integrated tool made from Vaisala that generates the ABLH from the Carrier-to-Noise ratio (CNR) and vertical velocity gradients. Evaluating this difference between measurement and model helps understand how these models could be corrected by on-site measurements for improved representation in wake modelling.

The following section in the introduction outlines the principles of the boundary layer, as this definition becomes relevant for the boundary layer retrieval method for the lidar and models. This report is then structured by first detailing the methodology, presentation of results, a discussion of the analysis, and key takeaways. Firstly, the methodology of the analysis is detailed: what datasets were used, both model and lidar ABLH derivation, and key performance indicators used to analyze the bias of ABL model and measurement and sensitivity analysis of the bias compared to dataset characteristics and atmospheric conditions. The results are presented and discussed in three parts. First, the overall ABLH distributions of the WRF, ERA5, and lidar are separately presented to obtain insight into the spread of data. Second, a direct comparison of bias and root mean square error (RMSE) is conducted to assess over or underestimation and the magnitude of the differences. Last, a sensitivity study is conducted by classifying these key performance indicators such as hour of the day, sea surface temperature, and others. The analysis concludes by summarizing the model performance compared to the lidar ABLH measurements and recommendations for model correction techniques.

1.1 Boundary layer definition

The ABLH is defined as the lowest portion of the troposphere that is most affected by the presence of surface forcings such as friction, pollution, heat transfer, etc (Stull, 1988). This area of the atmosphere is characterized by complex turbulent and temperature gradient processes, a unique challenge for determination from measurements (Puccioni et al., 2024). The boundary layer can be categorized in two ways: the mixing layer, defined by convective conditions and turbulent driven, and the residual layer, based on neutral or stable conditions. The residual layer is defined by aerosols driven not by convection but rather by passive atmospheric transport (Stull, 1988). These aerosols are called "tracers", and are important as lidars rely on these aerosols to obtain a return signal and perfectly follow the wind speed and direction. Figure 1 shows this distinction on a diurnal cycle. The mixing layer height is determined by convection and is mostly characterized by turbulent wind profiles. The residual layer is defined by more stable conditions and mostly during night, so the aerosols that were mixed in the atmosphere during the day remain aloft and act as tracers for any wind advection.

https://doi.org/10.5194/wes-2025-155
Preprint. Discussion started: 20 October 2025

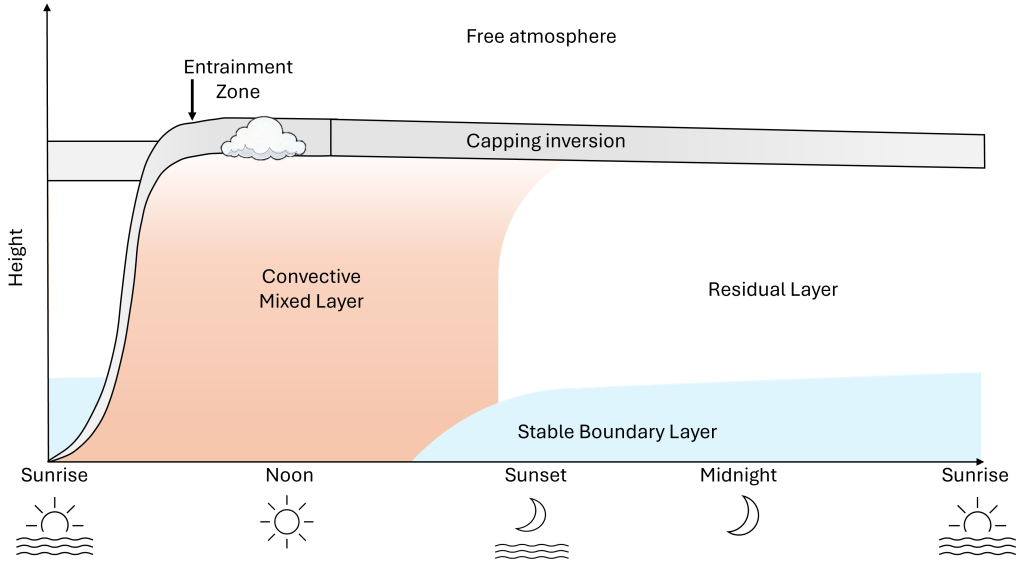

Figure 1. Graphic demonstrating the diurnal boundary layer development and distinction of the mixing and residual layer over the course of the day.

2 Methodology

2.1 Datasets

Two offshore campaigns were chosen for this analysis that include long term scanning lidar data and WRF ABLH simulations. Figure 2 shows the location of both campaigns in the North Sea. The GLOBE dataset is located completely offshore and the FLOW dataset was taken along the coast of northern Denmark.

The first campaign was funded by the X-Wakes project to participate in the Carbon Trust Offshore Wind Accelerator (OWA) Global Blockage Effect in Offshore Wind campaign (GloBE). Seven long range scanning lidars, in addition to various other instruments, were deployed on wind turbine transition pieces offshore to measure the global blockage effect on an offshore wind farm cluster in stably stratified conditions (Adams et al., 2023). One WindCube Scan (WCS) 200S lidar was reserved for making boundary layer measurements, Table 1 outlines the scanning strategy of the scanning lidar. The scanning strategy alternated from a two-minute fixed scan measuring completely vertically followed by 18 minutes of a Velocity Azimuth Display (VAD) scan which provides a reconstructed vertical wind speed profile. Only the ABL scan was used for this analysis. Figure 3 demonstrates the layout of the wind farms, location of the scanning lidar, meteorological mast, WRF cell size, and other floating lidar systems around the area.

The second campaign comes from the Flow, Loads and pOwer for Wind energy (FLOW) project, a research effort to develop and improve wind energy engineering applied models from in-situ data (Patel et al., 2025). This particular site, located on

https://doi.org/10.5194/wes-2025-155
Preprint. Discussion started: 20 October 2025

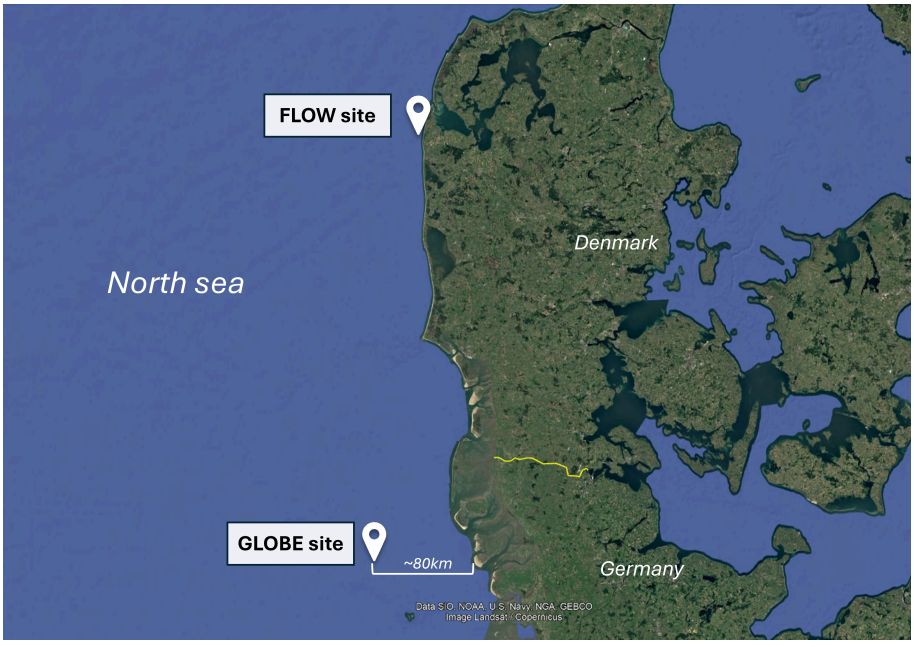

Figure 2. Map showing two offshore locations for the FLOW and GLOBE campaign

Table 1. GLOBE scanning strategy for the scanning lidar

Scan Name	Scan Type	Duration [min]	Elevation [°]	Accumulation Time [ms]	Pulse length [m]	Min Range [m]	Max Range [m]	Display Range [m]
ABL	Fixed	2	90	1000	50	100	7200	25
VAD	VAD	18	75	1000	50	100	6950	25

the coast of northern Denmark, also hosts multiple lidars conducting dual doppler scanning techniques to measure turbulence measurements. A WCS 200S lidar alternated from doppler beam swinging (DBS) for horizontal wind speed retrievals and a fixed vertical scan to measure the boundary layer height. Table 2 demonstrates the detailed scanning strategy for this lidar. Figure 4 shows the location and image of the lidar used, as well as the other lidars and a ceilometer on-site.

Table 2. FLOW scanning strategy for the scanning lidar

Scan Name	Scan Type	Duration [s]	Elevation [°]	Accumulation Time [ms]	Pulse length [m]	Min Range [m]	Max Range [m]	Display Range [m]
VAD	PPI	480	45	1000	25	100	3075	25
ABL	Fixed	120	90	1000	25	50	3025	25

Both campaigns aim to better understand maritime atmospheric conditions for wind energy applications through comparison of models such as WRF to multiple on-site remote sensing measurements. Since both sites are located in the North Sea, the analysis will demonstrate the consistency of ERA5/WRF model performance against the vertically profiling scanning lidar

https://doi.org/10.5194/wes-2025-155
Preprint. Discussion started: 20 October 2025

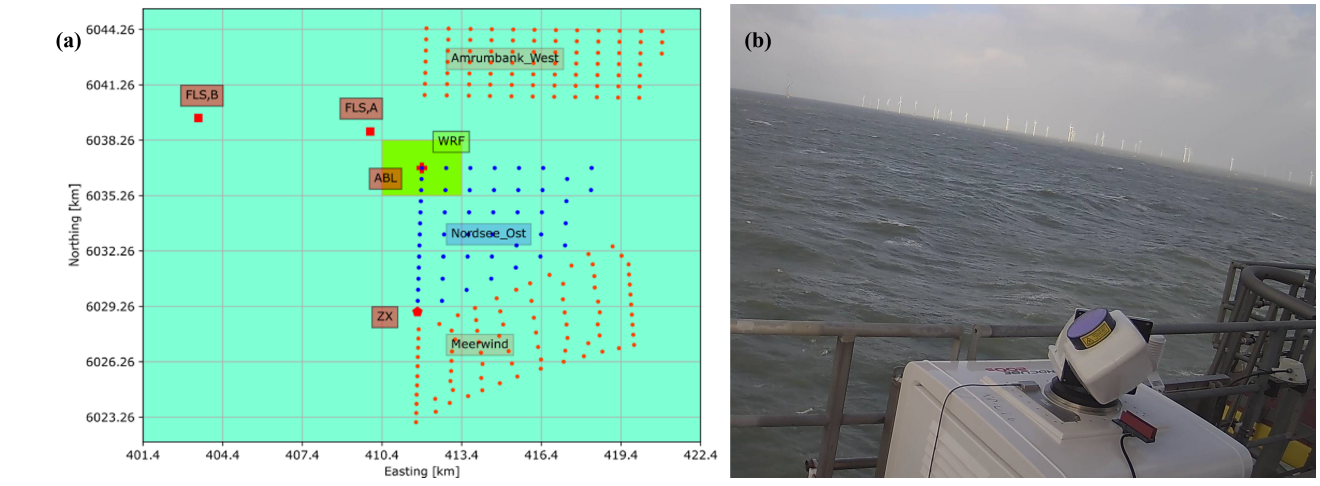

Figure 3. This figure was taken from Adams et al. (2023). Graphic (a) shows a detailed map demonstrating the GLOBE campaign scanning lidar location (labeled "ABL") and surrounding offshore wind farms in the North Sea. The scanning lidar was placed on the platform of the meteorological (met) mast. The wind farms are located north, south, and west of the lidar. Graphic (b) shows the scanning lidar's "view" of the wind farms from the met mast platform.

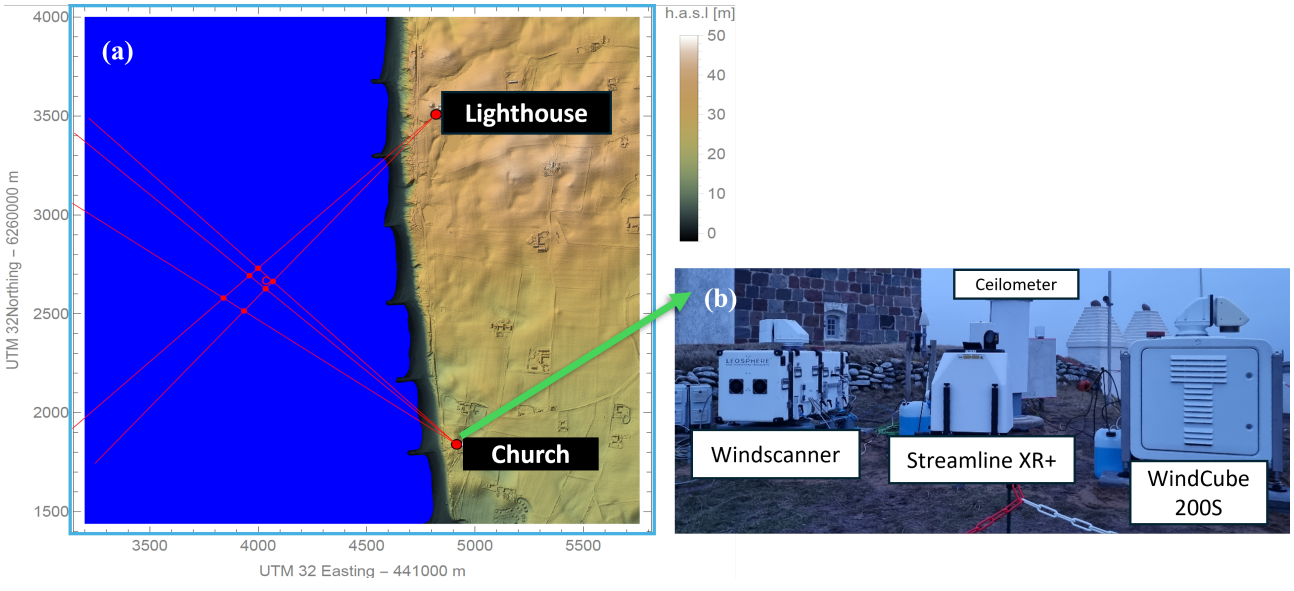

Figure 4. Graphic (a) shows the dual-doppler scanning strategy for the FLOW campaign on the coast of Denmark. This analysis focuses on the scanning lidar measurements done at the church site by the WindCube 200S, as seen in graphic (b) with other measurement devices.

measurements. Additionally, as the GLOBE site is located completely offshore and the FLOW site directly on the coastline, this study aims to evaluate if the sensitivity of measurement/model bias is dependent on location and surface roughness. Table 3

https://doi.org/10.5194/wes-2025-155
Preprint. Discussion started: 20 October 2025

provides detailed information on each campaign. The additional sensors for the GLOBE site are attributed to the meteorological mast that is located on site.

Table 3. FLOW and GLOBE campaign descriptions

Name	Coordinates	Start Date	End Date	Duration	Instrumentation on site
GLOBE	[54.47 , 7.64]	08/2021	04/2022	9 months	– WindCube Scan 200S lidar – Sonic anemometers (32m and 92m) – Wind vanes (32m and 92m) – Sea surface temperature sensor
FLOW	[56.51 , 8.09]	02/2024	06/2024	5 months	– WindCube Scan 200S lidar – CL51 Ceilometer

2.2 ABL Estimates

The following subsections detail the method to derive ABLH from both the lidar return signal and vertical velocities, as well as the averaging methods used to be comparable to the temporal scale of the mesoscale models.

2.2.1 Lidar ABLH Detection

The WindCube Scan has an integrated algorithm that takes as input the CNR and vertical velocity and outputs the ABLH. The radial wind speed denotes the value of the wind speed moving towards or away from the lidar beam, so when measuring vertically this is the vertical velocity. Since the mixing layer height is characterized by turbulence, the standard deviation of the vertical velocity is calculated to estimate the vertical turbulence (Flamant et al., 1997). The vertical turbulence gradient is then evaluated to determine the height of the convective layer. The CNR represents an indicator of the lidar's return signal strength based on aerosol concentration. In the residual layer, aerosols behave as passive tracers in these conditions, so the vertical CNR gradient is used as an indicator of aerosol dispersion within the boundary layer (Bianco and Wilczak, 2002) (Bianco et al., 2008).

Figure 5 demonstrates the general workflow of the ABLH algorithm. The vertical gradients of the radial velocity and CNR are used to generate the mixing and residual layer, respectively. Both variables are filtered using a confidence index ("Status IC" in the figure) to remove invalid data. The gradients of these variables along the line of sight are calculated. The distribution of these gradients as a function of height is assessed for local maxima and minima through a series of logic analysis to determine the boundary layer height. A cloud height detection algorithm is used to properly define the boundary layer height: in some cases, the height is determined as the cloud base, and if there are multiple clouds then the height is determined as the maximum of the local gradients. The latitude, longitude, and timestamp are used to determine sunrise and sunset times to characterize the mixing and residual layer heights. These steps are applied for a specific averaging window, in this project set to 30 seconds.

https://doi.org/10.5194/wes-2025-155
Preprint. Discussion started: 20 October 2025

eawe european academy of wind energy
Open Access WIND ENERGY SCIENCE DISCUSSIONS

For each window, the output of the algorithm includes the residual layer height, the mixing layer height, the cloud base height. Figure 6 displays a sample output of mixing and residual layer heights for an extended time period, demonstrating accuracy in well defined boundary layer conditions.

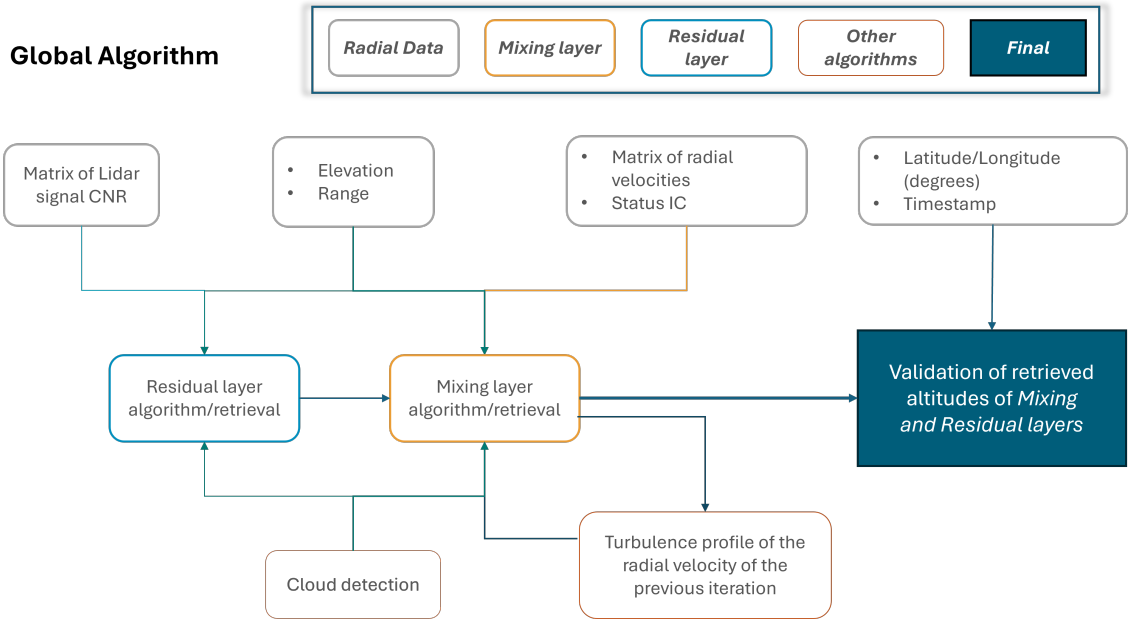

Figure 5. ABL detection flowchart outlining the steps necessary to calculate the residual and mixing layer.

A final logical decision tree is applied to the residual and mixing layer heights to ensure the values are physically logical. For example, all mixing layer heights generated in the middle of the night must not be considered as convective conditions do not exist.

ERA5 data is originally outputted on an hourly basis, so the WRF and lidar datasets were averaged to accomodate this temporal resolution.

The lidar outputs both residual and mixing layer heights at some parts of the day and data is provided every 30 seconds, so three averaging methods were conducted to assess the sensitivity of evaluating the ABLH in different conditions. Averaging both ABLH retrieval types results in an ABLH that is not representative of the true conditions. The three averaging methods are defined in Table 4: the residual layer average, where only the residual layer retrievals are considered, the mixing layer average, and a "time of day" (ToD) average. This method assumes that the boundary layer is defined by the diurnal cycle, where only the mixing layer is considered during daytime hours, the residual layer during nighttime hours, and an average of both around sunset and sunrise hours.

https://doi.org/10.5194/wes-2025-155
Preprint. Discussion started: 20 October 2025

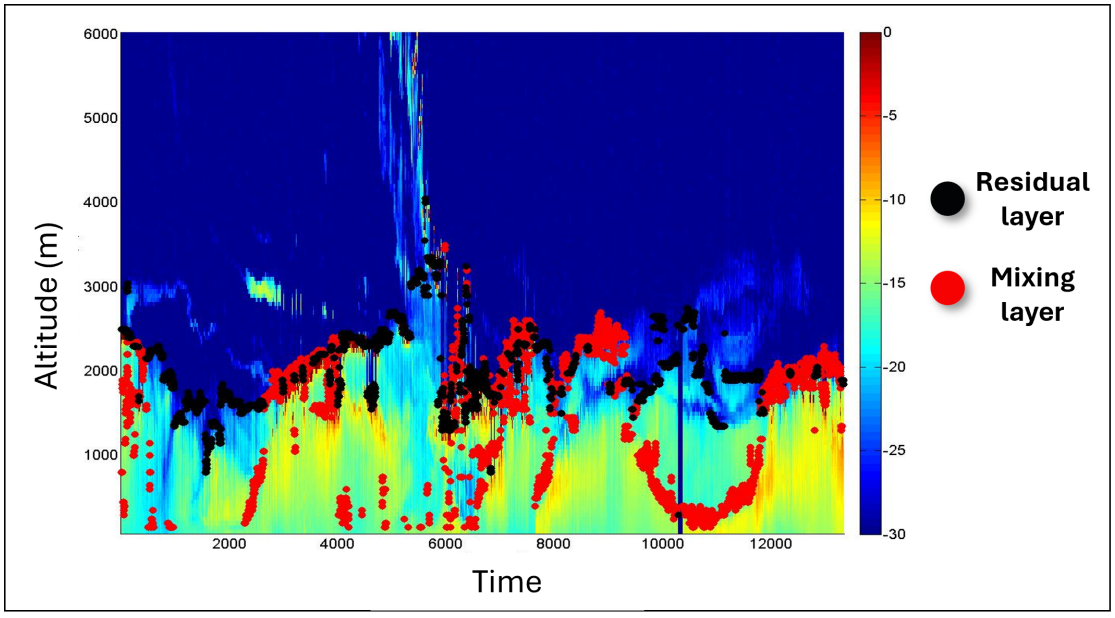

Figure 6. Visual representation of residual and mixing layer heights. This example comes from a sample dataset from the validation of the tool, the timeline shows 24h on the x axis with colors demonstrates a range of the CNR.

Table 4. Description of three averaging techniques for lidar ABLH retrievals of mixing and residual layer heights.

Name	Abbreviation	Meaning
Mixing Layer	Mix	Only mixing layer ABLHs are averaged
Residual Layer	Res	Only residual layer ABLHs are averaged
Time of Day	ToD	Only mixing layer averaged during daytime; only residual layer averaged during nighttime; both are averaged $\pm$ one hour from the sunrise/sunset time

2.2.2 ERA5 ABLH

The ERA5 Reanalysis product provides atmospheric data from a model informed by observational data on a global scale. It is the 5th generation of atmospheric reanalysis to be produced by ECMWF, with hourly resolution output of 0.25° (Hersbach et al., 2020). As ERA5 is based on observational datasets, the preceding method for measuring the ABLH and its characteristics is done with radiosondes as these instruments provide temperature, humidity, and pressure data below and above the ABL. ERA5 uses the Bulk Richardson number to determine the ABLH as it has been found to provide the overall best representation for stable and convective boundary layers not highly dependent on sounding vertical resolution in a study conducted by Seidel et al. (2012) and Vogelezang and Holtslag (1996). Equation (1) shows the Bulk Richardson calculation (R_i),

https://doi.org/10.5194/wes-2025-155
Preprint. Discussion started: 20 October 2025

eawe european academy of wind energy
Open Access WIND ENERGY SCIENCE DISCUSSIONS

$$R_i(z) = \frac{(g/\theta_{vs})(\theta_{vz} - \theta_{vs})(z - z_s)}{(u_z - u_s)^2 + (v_z - v_s)^2} \quad (1)$$

R_i represents the ratio of turbulence associated with buoyancy to turbulence associated with mechanical shear. The numerator, representing buoyancy, is a function of gravity g, height z, surface height z_s, and virtual potential temperature θ_{vs}. The denominator, representing shear, is composed of the sum of the squares of the differences between surface and elevated velocity components u and v.

Seidel et al. (2012) note that a Bulk Richardson number of 0.25 indicates the top of the boundary layer. Vogelezang and Holtslag (1996) find that the ABLH characterized by the Bulk Richardson value performs well over land but in areas with high wind speeds over the ocean where deep boundary layers may arise, R_i may not capture extreme ABL conditions. The lack of literature pertaining to validation of this method, which is applied in ERA5 and other models, leads to an opportunity for scanning lidars to provide direct measurements of stability conditions and height variation of the ABLH.

2.2.3 WRF

The WRF parameterizations used in this analysis are based on the research done in Cañadillas et al. (2022), where scanning lidars were used to quantify cluster wake effects in the German Bight region. The results demonstrated good agreement of wake effects from both the model and scanning lidar measurements in neutral and unstable conditions. Stable conditions yielded the largest discrepencies, between 10-20% disagreements in wind speed. Though this analysis focuses on ABLHs, this provides an indication that stable conditions with these parameterizations are not well simulated. Additional studies using MYNN support this results. Sandu et al. (2013) concluded that increased turbulence diffusion in ABL schemes increases precision for surface temperature at the cost of inducing extra mixing. Olson et al. (2019) found similar results of increased mixing in stable conditions, thus providing a basis for a misrepresentation in heat flux parameterization driving the turbulence diffusion.

The WRF dataset assessed in this study already includes the location of the scanning lidar used in this study. The same parameterizations were used to rerun the WRF simulation for the FLOW site, as seen in Table 5. The Mellor-Yamada-Nakanishi-Niino (MYNN) level 2.5 boundary layer scheme was used, as well as ERA5 data used for atmospheric boundary layer conditions. The horizontal resolution is 2km.

2.3 Presentation of applied metrics

The comparative results are presented in three parts: lidar vs. WRF/ERA5 ABLH distribution, lidar vs. WRF/ERA5 ABLH direct comparison, and a sensitivity analysis.

First, the ABLH distributions from the lidar, WRF, and ERA5 are presented separately by probability density distributions for the overall campaign from each dataset.

Second, two key performance indicators (KPIs) are used to compare lidar and model ABLH derivations: bias and root mean square error (RMSE). A simple mean bias error calculation, as seen in (2) was used to assess the positive and negative tendencies of the lidar measurements as compared to the ERA5/WRF outputs,

https://doi.org/10.5194/wes-2025-155
Preprint. Discussion started: 20 October 2025

eawe european academy of wind energy
Open Access WIND ENERGY SCIENCE DISCUSSIONS

Table 5. Description of WRF parameterizations used in this study. The same setup was using in Cañadillas et al. (2022)

Parameter	Setting
WRF model version	4.2.1
Atmospheric boundary layer (ABL) scheme	MYNN level 2.5
Wind farm parameterization	Fitch et al. (2012)
Land use data	MODIS
Surface layer scheme	MYNN
Mucrophysic scheme	WRF single-moment five-class
Shortwave and long-wave radiation	RRTMG
Atmospheric boundary conditions	ERA5
Sea surface conditions	OSTIA
Horizontal resolution	18, 6, 2km
Vertical resolution	60 eta level
Nudging	Grid nudging above ABL
Model output interval	10 min
Nesting	One-way
Land surface model	Unified Noah Land Surface Model
Simulation suration	240 (+24 spin up) hours

$$\text{Bias} = \frac{\sum_{i=1}^{N} h_{model}(i) - h_{lidar}(i)}{N} \tag{2}$$

where h_{model} represents the ABLH derived from the model and h_{lidar} that of the lidar in the same hour timeframe. Equation (3) demonstrates the RMSE,

$$\text{RMSE} = \sqrt{\frac{\sum_{i=1}^{N} |h_{model}(i) - h_{lidar}(i)|^2}{N}} \tag{3}$$

where N is the population size. This becomes more relevant during the sensitivity study where the datasets are sorted by varying distributions based on hour of the day, month, temperature, and other variables.

Last, a sensitivity analysis is conducted. The bias and RMSE are then categorized by bins of different atmospheric and temporal conditions to assess if observational/model ABLH values are sensitive to specific conditions. Table 6 outlines the variables used in the sensitivity study. The Monin-Obhukov length (MOL) is analyzed for the GLOBE site thanks to the availability of the appropriate sensors to capture and calculate these variables. Table 7 outlines the categorization of stability conditions based on the MOL values. The sea surface temperature (SST) bias between the measured SST onsite and from the

https://doi.org/10.5194/wes-2025-155
Preprint. Discussion started: 20 October 2025

eawe european academy of wind energy
Open Access WIND ENERGY SCIENCE DISCUSSIONS

model is also used as a sensitivity variable to find a correlation with ABLH bias and potential sources of heat flux deviation from real conditions.

Table 6. Sensitivity variables analyzed for the GLOBE and FLOW campaign

Variable	**GLOBE**	**FLOW**
Hour of Day	Lidar timestamp	Lidar timestamp
Month	Lidar timestamp	Lidar timestamp
Wind direction	Wind vanes	Lidar DBS
SST bias	Temperature sensors	
MOL (stable, unstable, neutral)	Sonic anemometers	

Table 7. MOL stability categorization

Condition	**Stability case**	**Abbreviation**
MOL $\leq$ -0.25	Unstable	1_U
-0.25 > MOL $\leq$ -0.05	Near Unstable	2_NearU
-0.05 > MOL $\leq$ 0.05	Neutral	3_N
0.05 > MOL $\leq$ 0.25	Near Stable	4_NearS
MOL > 0.25	Stable	5_S

3 Results and Discussion

3.1 Visualization of results

Figures 7 and 8 show a sample of the lidar ABLH retrievals for the GLOBE and FLOW datasets, respectively. Often the boundary layer conditions are clearly delineated. These two cases demonstrate conditions where the boundary is vague. Figure 7 shows a clear mixing layer height from the vertical velocity around 400 m, yet the CNR gradient drops off at a much greater height around 2 km, which leads to a disagreement with the single boundary layer definition from the models. The mixing layer height is closer to the model output, and the ToD average method would only include this value in the hourly average. Figure 8 shows a residual layer height only slightly higher than the mixing layer height. As the boundary layer height is difficult to quantitatively validate, these case studies show the visual interpretation and verification of the lidar ABLH retrieval method. This qualitative analysis is often done for boundary layer measurements from remote sensors (Liu and Liang, 2010) (Jozef et al., 2022). Analysis of sufficient examples ultimately provide an acceptable level of confidence for the ABLH retrieval from the scanning lidar.

https://doi.org/10.5194/wes-2025-155
Preprint. Discussion started: 20 October 2025

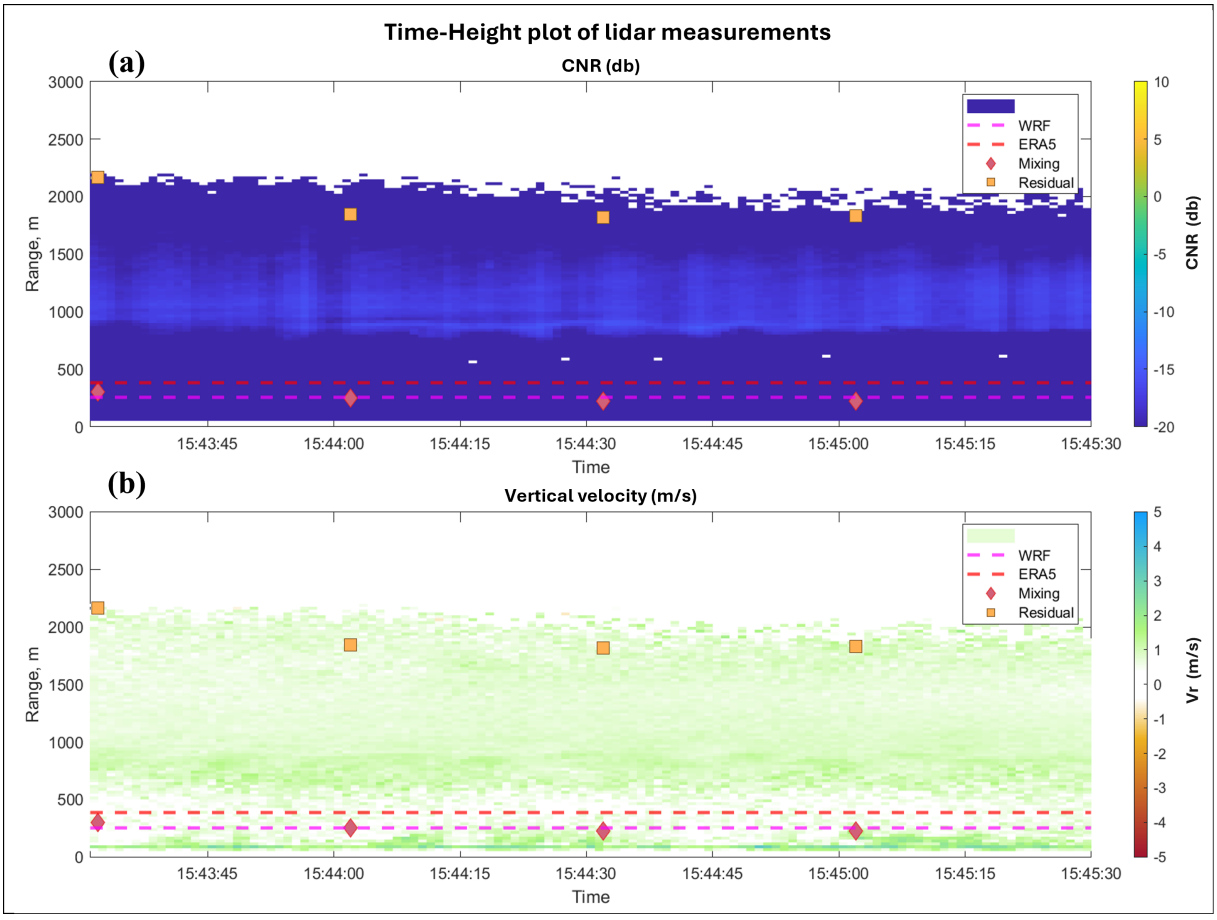

Figure 7. The figure demonstrates a time/height plot from the lidar CNR in (a) and vertical velocity in (b) from the GLOBE dataset, taken from March 13th 2022 from 15h43-15h45. The x axis denotes the passage of time and the y axis the altitude in the vertical direction. The variables are color coded to denote intensity of their magnitude. The mixing layer is denotes as a red diamond, and the residual layer as an orange square.

3.2 ABL lidar distribution

Figure 9 demonstrates the probability distribution function (PDF) of the ABLHs derived from WRF, ERA5, and the three different averaging techniques from the lidar.

Both sites demonstrate similar distribution characteristics for the mixing, residual, and ToD average lidar ABLH retrieval. The mixing layer heights generate a higher density of lower ABLHs, whereas the residual layer heights demonstrate a more well-spread distribution of both low, medium, and high altitudes for the ABLH. The ToD, as it considers both mixing and residual on a diurnal basis, shows a balance between the two. Since the mixing layer represents the height of the atmosphere

https://doi.org/10.5194/wes-2025-155
Preprint. Discussion started: 20 October 2025

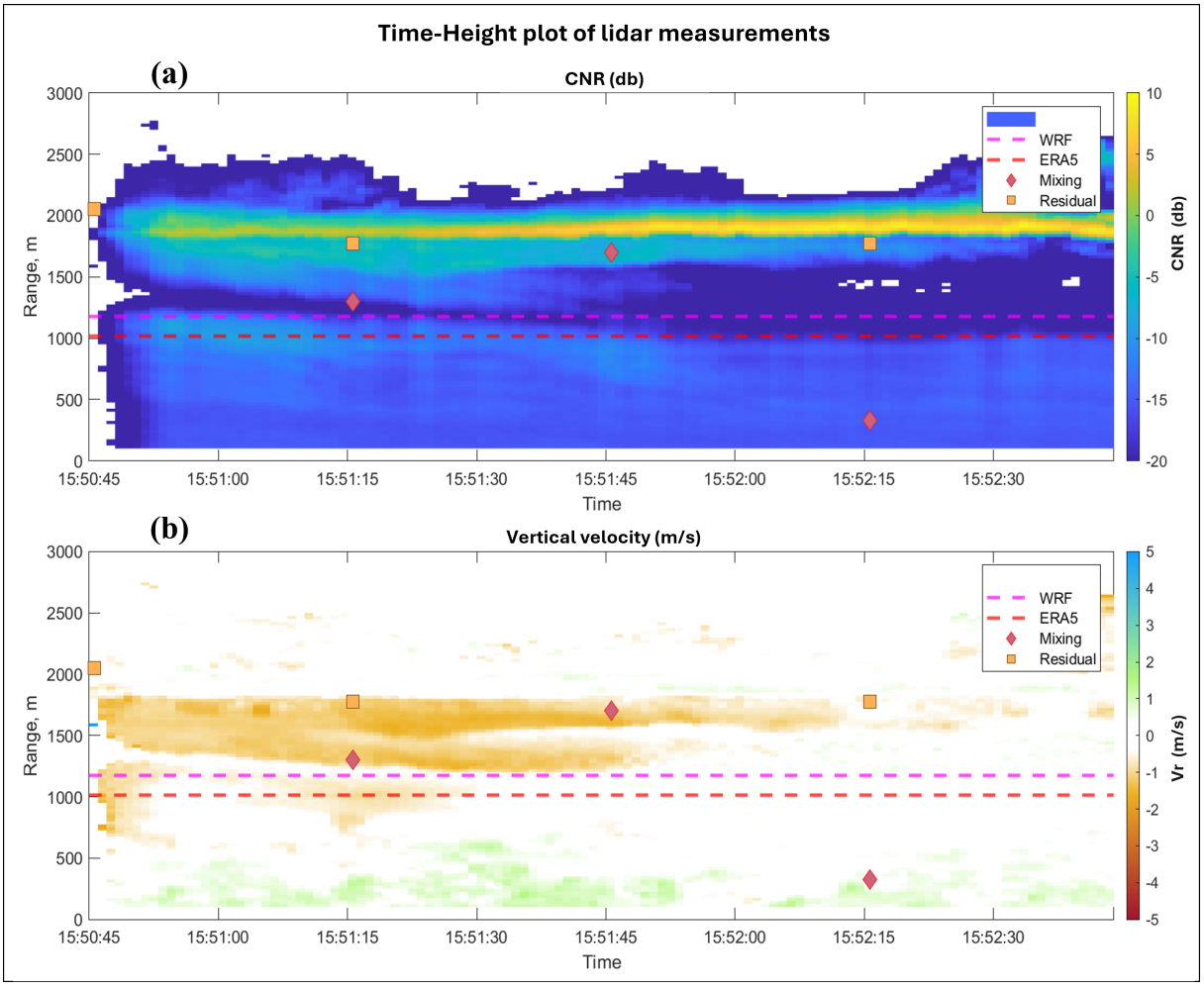

Figure 8. The figure demonstrates a time/height plot from the lidar lidar CNR (a) and vertical velocity (b) plot from the FLOW dataset, taken from March 21st 2022 from 0h20 to 0h22.

based on convective activity, i.e. turbulence, this gradient threshold is almost always below the aerosol concentration dropoff which defines the residual layer.

The comparison of the model ABLHs with the lidar measurements shows overestimation by the models. Based on the particular atmospheric conditions of the site, both the reanalysis and mesoscale model do not capture the prevailing low ABLH conditions, demonstrated at least 15% of the time to be 100m from the lidar ABLH measurements and only between 2-4% from the models.

The FLOW site demonstrates a wider range of ABLHs compared to GLOBE. The lidar ABL measurements show a more even distribution across all heights between 100-2000m, with probability of 2km heights from residual layer measurements

https://doi.org/10.5194/wes-2025-155
Preprint. Discussion started: 20 October 2025

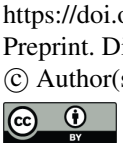

eawe european academy of wind energy
Open Access WIND ENERGY SCIENCE DISCUSSIONS

265 reaching around 12%. The model ABLH distribution, however, drops off at around 1400m, meaning the models rarely output ABLHs above this value.

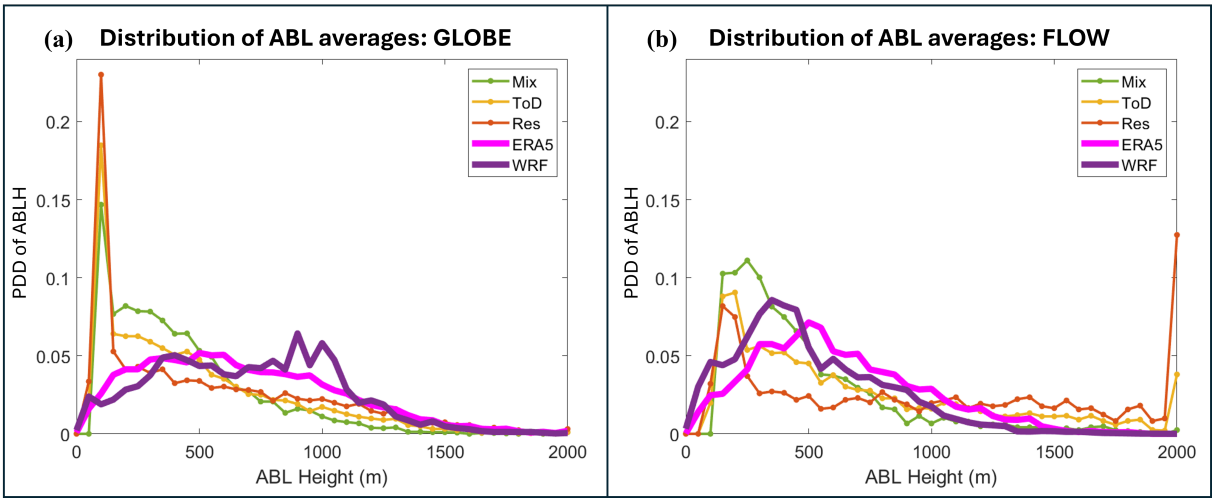

Figure 9. Probability density distribution (PDD) of the ABLH from all three lidar averages, WRF, and ERA5. Figure (a) shows the ABLH dataset distribution from the GLOBE site, and figure (b) from the FLOW site.

3.3 Assessing bias and RMSE

Figure 10 demonstrates the bias (model ABLH – lidar ABLH) for the GLOBE (left) and FLOW (right) datasets.

For the GLOBE site, the model comparison to all lidar averaging techniques demonstrate an overestimation from the model 270 ABLH. The WRF model data tends to perform slightly better than ERA5, with the residual layer average yielding the lowest bias. The biases for each model range from 184-348m for WRF and 231-422m for ERA5. This is significant for the GLOBE site where ABLH conditions are typically around 100-400m based on the distribution graph. If the actual ABLH conditions are 100m and the model normally overestimates by 300m, the wake dissipation may be stronger than real ABL conditions will allow.

275 The bias results for the FLOW site are significantly different from the GLOBE dataset. The mixing layer average of the lidar ABLH measurements yield small, positive bias. The time of day and residual layer averages, however, demonstrate an underestimation from the model, with extreme biases from the residual layer average between 557 and 458m difference from WRF and ERA5, respectively. Thus, this extreme overestimation needs further investigation on both the model and lidar side to assess the validity of the ABLH measurement.

280 Figure 11 shows the root mean square error (RMSE) between the model ABLH output compared to the measurements.

The RMSE for the GLOBE dataset yields very similar results among all the lidar ABLH averaging techniques and WRF/ERA5. The mixing layer height yields the lowest RMSE with values around 370m from WRF and ERA5, whereas the residual layer height is around 470m. These results contrast the previous bias analysis, where the residual layer yielded lower

https://doi.org/10.5194/wes-2025-155
Preprint. Discussion started: 20 October 2025

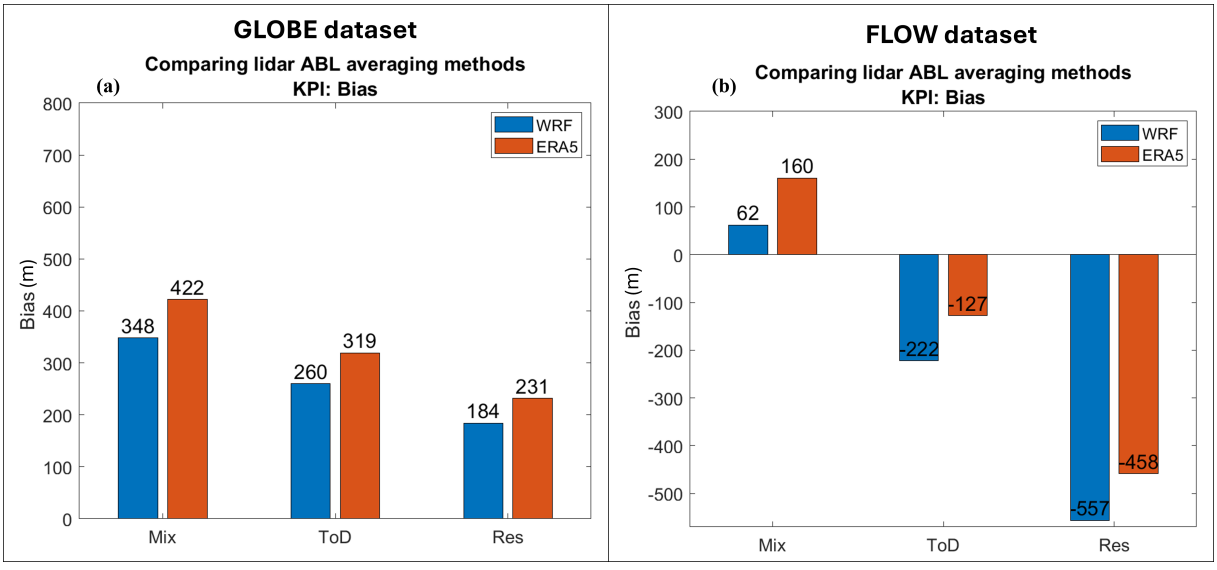

Figure 10. ABLH bias results for all three lidar averaging techniques. Each grouping represents a lidar averaging technique, and each color represents WRF/ERA5 (blue and red, respectively). Figure (a) shows the results for the GLOBE dataset, and figure (b) for the FLOW dataset.

biases. The residual layer bias is more variable, sometimes underestimating. ERA5 performs slightly better than WRF, contrasting with the WRF performance for the bias.

The RMSE of the FLOW dataset demonstrates similar results as the previous section, with the residual layer ABLH yielding the most extreme results. The comparison of the mixing layer retrieval to the models yields an RMSE of around 300m for both models, where WRF performs slightly better than ERA5. The ToD and residual layer lidar retrievals, however, yield a significantly higher error of around 600m for ToD and around 750m for the residual layer. This variability in the comparison of different lidar ABLH definitions shows the importance of how the ABLH is characterized. The disparity between the models and lidar measurement demonstrate a great distrinction between the ABLH definition based on turbulence or concentration of backscatter.

3.4 Sensitivity analysis

Figure 12 and Figure 13 demonstrate the distribution of all the sensitivity variables for each of the model data comparisons. The wind direction is predominantly east and south easterly, which may indicate turbine wake effects in the wind speed; the lidar measurements measure the wake while the models do not include wakes. The SST bias represents the difference between the SST generated by the model from the SST measured on the GLOBE site. The SST bias is slightly skewed with a bias centered around 1° overestimation from the models. The MOL bias is not well distributed, demonstrating extreme conditions between stable and unstable conditions. The FLOW sensitivity variable dataset distribution seen in Figure 13 shows slightly more stable distributions, with limited data with northerly wind directions but otherwise well dispersed data.

https://doi.org/10.5194/wes-2025-155
Preprint. Discussion started: 20 October 2025

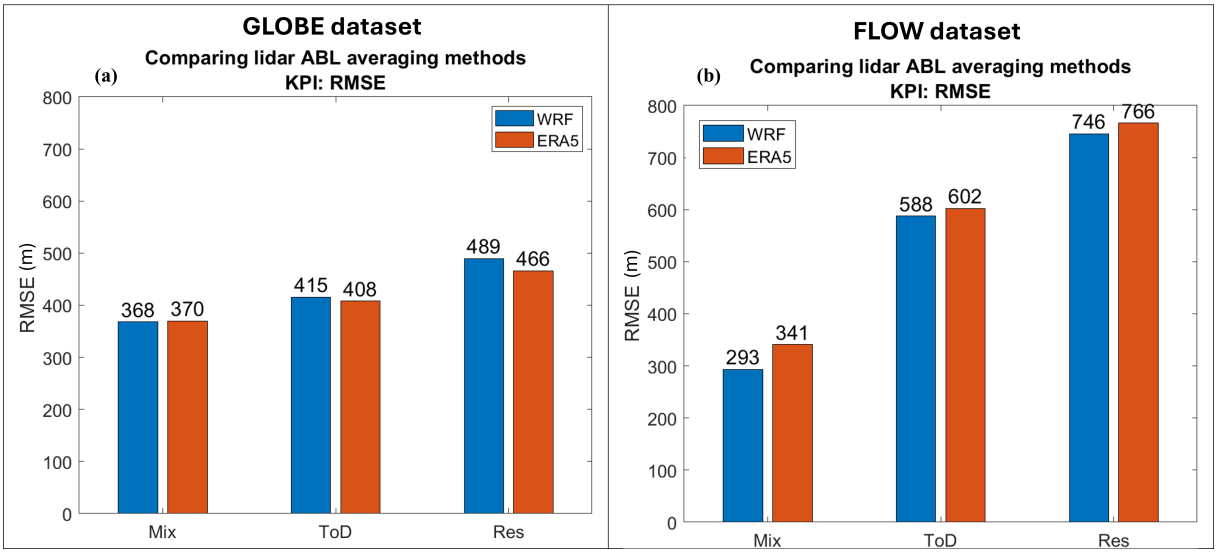

Figure 11. ABLH RMSE results for all three lidar averaging techniques. Each grouping represents a lidar averaging technique, and each color represents WRF/ERA5 (blue and red, respectively). Figure (a) shows the results for the GLOBE dataset, and figure (b) for the FLOW dataset.

3.4.1 Hourly sensitivity

The hourly sensitivity to the WRF/ERA5 bias can be seen in Figure 14. For the GLOBE dataset, the bias varies significantly, from an overestimation of 70m from the residual layer average and 506m overestimation from the mixing layer average. The RMSE varies from 385m from the mixing layer average and the highest from the residual layer average at 590m. For both bias and RMSE the best agreement occur in the middle of the day, whereas the bias and RMSE slightly increase during nighttime hours. As the ToD average is based on the mixing/residual average values based on the time of day, this average method shows the highest sensitivity to the diurnal cycle. Regarding model performance, both models yield an overestimation compared to the measurements. WRF yields lower bias results compared to ERA5, and performs slightly better than ERA5 in the RMSE results.

The FLOW dataset shows more disagreement in bias and RMSE. The mixing layer bias ranges from 0 to 270m overestimation for both models, whereas the residual layer bias shows an underestimation between -270m to -700m. The RMSE is similarly high for the residual layer average, fluctuating between 700-1000km difference with the measurements. The mixing layer average is significantly lower, ranging from around 160m-400m. Similarly to the GLOBE dataset, there is a slight diurnal sensitivity for both bias and RMSE. For this dataset, WRF demonstrates better results for bias and RMSE when compared with the mixing layer average and ERA5 with the residual layer average.

Figure 15 shows monthly sensitivity plots of hour of day versus ABLH bias for the GLOBE and FLOW datasets. The lidar ABLH average assessed in this graph is the ToD to a more accurately evaluate boundary layer conditions. The GLOBE dataset

https://doi.org/10.5194/wes-2025-155
Preprint. Discussion started: 20 October 2025

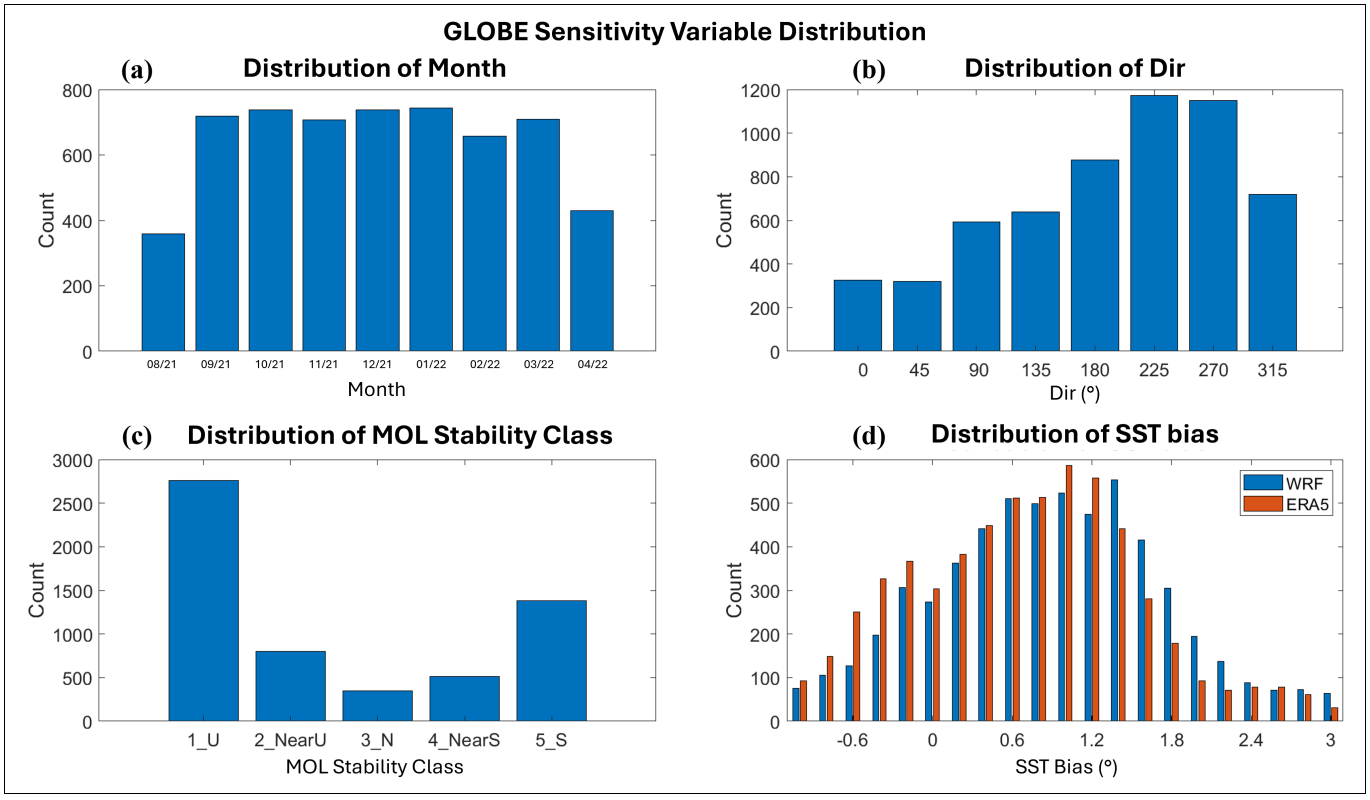

Figure 12. Histograms of all sensitivity variables assessed for the GLOBE dataset: month of the year (a), wind direction (b), MOL stability classifiction (c), and SST bias (d). The "count" denotes the data point counts for each bin of the specific variable.

demonstrates slightly worse performance from ERA5 compared to WRF, with overestimation from both models in all months except February and March. The diurnal cycle sensitivity is rarely present until February onwards, indicating a possible shift in the heat flux balance in the model representation. The FLOW dataset demonstrates more varied results, with more stable ABLH bias sensitivities in February and June and significantly pronounced biases in all other months. ERA5 shows slightly worse performance than WRF. The standard error (shaded area around the curves) for both datasets is relatively stable with ABLH bias fluctuating around 100m throughout the day.

3.4.2 Wind direction sensitivity

The wind direction sensitivity was evaluated to discern any correlation with specific site features that may not be captured in the WRF/ERA5. Figure 16 demonstrates the sensitivity results of bias and RMSE for the GLOBE and FLOW sites for each of the lidar averaging techniques. Recalling Figure 3 for the GLOBE site, there are wind farms located to the north, south, and east of the lidar. The results show a slight sensitivity and higher bias/RMSE to the northwesterly/northerly winds. The best performing bias and RMSE occur between the east/southerly winds, with a low of around 200m RMSE compared to the

https://doi.org/10.5194/wes-2025-155
Preprint. Discussion started: 20 October 2025

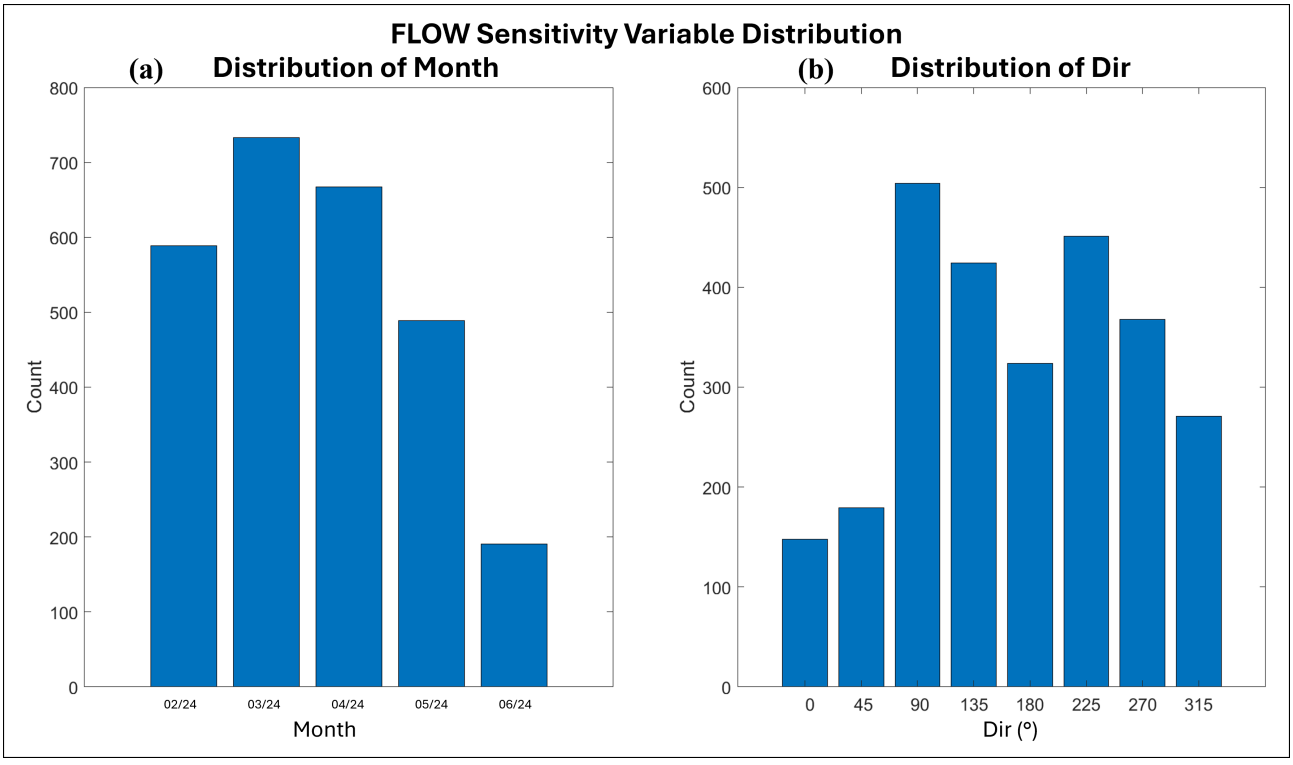

Figure 13. Histograms of all sensitivity variables assessed for the GLOBE dataset: month of the year (a) and wind direction (b). The "count" denotes the data point counts for each bin of the specific variable.

average 500m RMSE. This sensitivity could be due the lack of wake consideration in both models. Turbine wakes induce mixing thus increasing the entrainment layer and increasing the boundary layer height (Abraham et al., 2024). It is possible that the lower bias and RMSE in the east/southerly winds is not the models' accuracy in these wind direction bins, but rather the genuine conditions of increased boundary layer heights attributed to wakes.

The scanning lidar for the FLOW dataset is located along the coastline as seen in Figure 4, with the land on the eastern side and ocean on the western side. The relationship between the lidar averages and model appear to have a slight sensitivity to wind direction with lower bias and RMSE around the northwest/northerly wind direction bins. Though the residual and ToD lidar average methods yield extreme bias and RMSE results (up to 1km), they converge with low bias and RMSE values at these wind speed bins. This may indicate well represented conditions of northerly winds in the models, whereas the coastal flow on the eastern/western sides may not be well parameterized.

3.4.3 MOL sensitivity

The MOL sensitivity is demonstrated for the GLOBE dataset in Figure 17. The conditions are primarily unstable or stable. The sensitivity results in Figure 17 do not demonstrate any significant correlation of bias or RMSE to the stability characterizations

https://doi.org/10.5194/wes-2025-155
Preprint. Discussion started: 20 October 2025

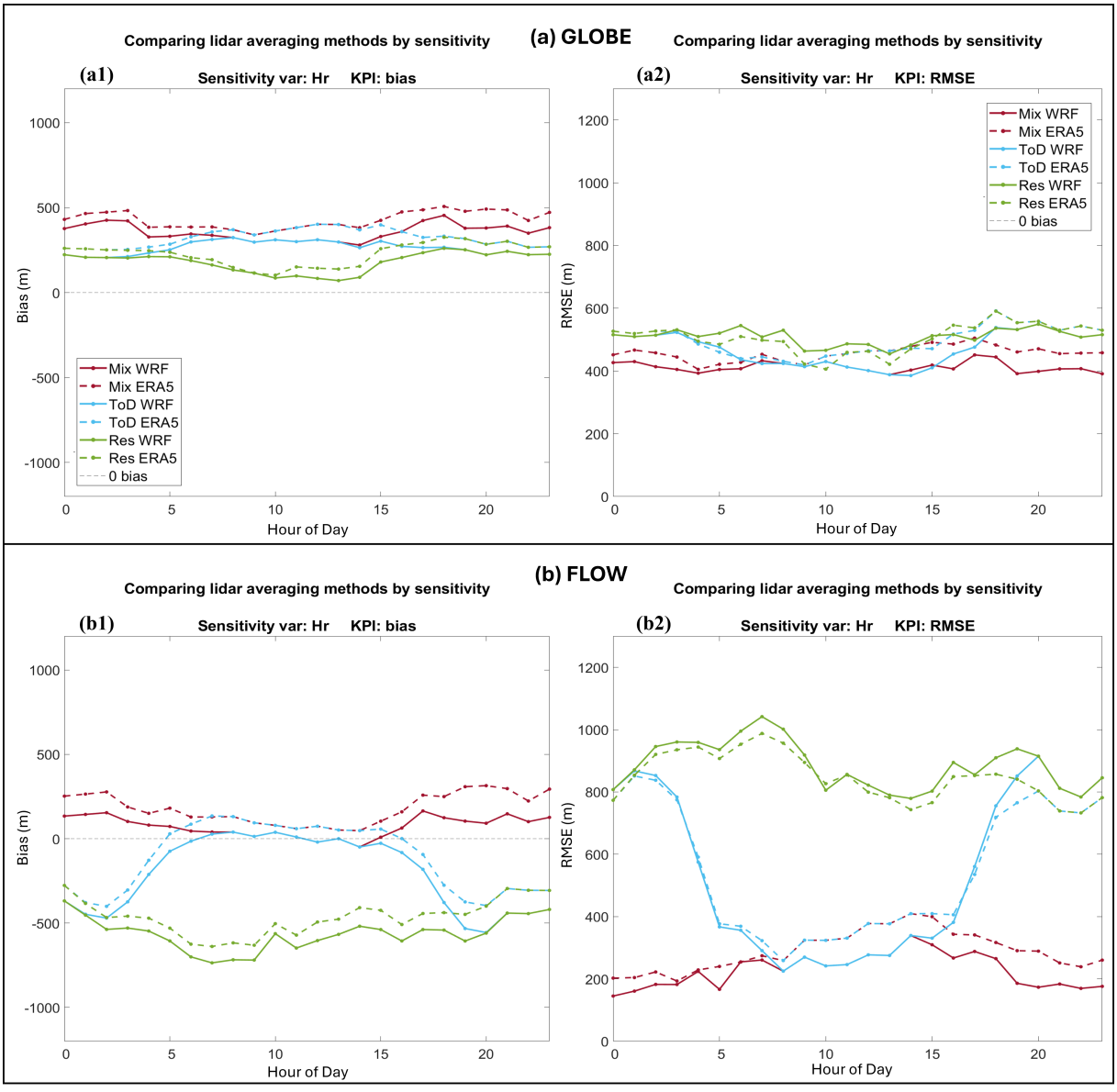

Figure 14. Hourly sensitivity graphs of average bias and RMSE for each hour of the day. Figure (a) shows the the results for the GLOBE dataset, demonstrating the average bias (a1) and average RMSE (a2) for each hour of the day. Similarly, (b1) and (b2) demonstrate the average bias and RMSE, respectively, for the FLOW dataset. The three colors indicate the three different lidar ABLH averaging techniques.

of the MOL. To continue investigating stability influences on the ABLHs, sea surface temperature was evaluated as a potential source of heat flux misrepresentation.

https://doi.org/10.5194/wes-2025-155
Preprint. Discussion started: 20 October 2025

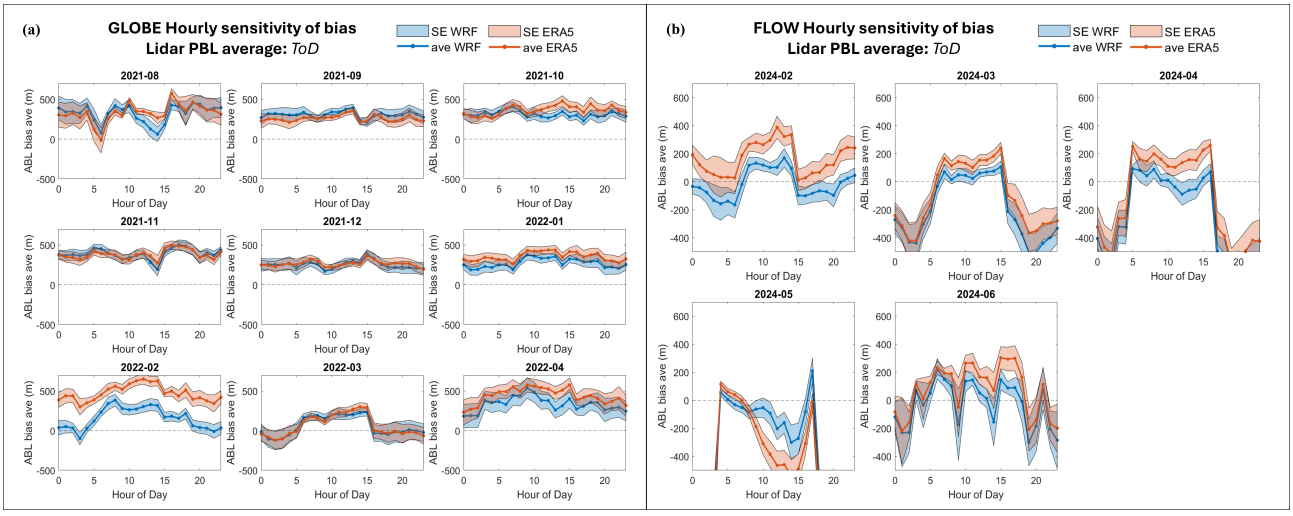

Figure 15. Hourly sensitivity graphs of hour of the day versus ABLH bias for each month of the campaign, plotted for the GLOBE campaign (a) and FLOW campaign (b). The shaded areas around the curves denote the standard error to evaluate variability around the sensitivity.

3.4.4 SST bias sensitivity

The SST bias from the onsite measurement and the models was calculated to assess potential correlation with the ABLH bias. Figure 18 shows a sensitivity of the WRF dataset to the SST bias, where a positive SST means an overestimation from the model. Both the ABLH bias and RMSE graphs demonstrate a positive correlation with the SST bias, meaning the greater the overestimation of SST from the models, the greater the bias and RMSE of the ABLH from both models. The ERA5 curves are relatively stable, fluctuating around a stable level of the average bias and RMSE.

4 Discussion

For both sites, the ABL lidar retrievals demonstrate tendencies of lower ABLHs with the mixing layer definition, and higher ABLHs with the residual layer definition. The difference between the mixing and residual layer average is much greater for the FLOW dataset, almost 500m difference in the RMSE when compared to the model difference. This indicates and confirms the model ABLH definition to be based on convective conditions, rather than the distribution of aerosols in the atmosphere.

The better performance from the mixing layer lidar measurement average can be attributed to the basis that the ABL in the models is also defined by turbulence characterizations. The WRF ABL scheme used in this analysis is based on an eddy diffusivity model which defines the turbulent kinetic energy (TKE) balance, stability equations, and mixing length. ERA5 is based on the Richardson number which is based on both potential temperature and wind speed gradients at difference heights. Because neither model defines the ABL by aerosol concentration, it is unlikely to agree with the residual layer definition from the lidar.

https://doi.org/10.5194/wes-2025-155
Preprint. Discussion started: 20 October 2025

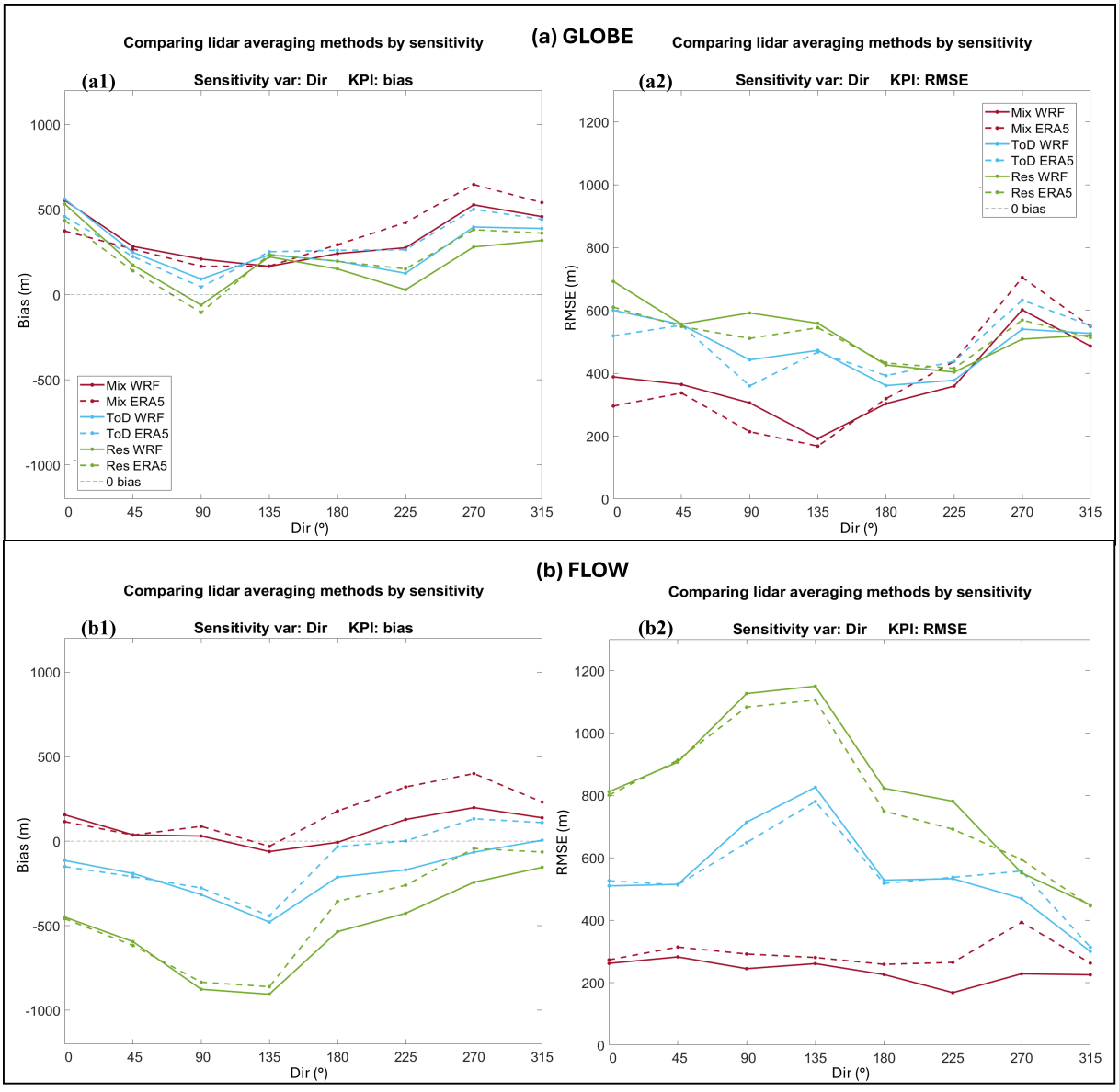

Figure 16. Wind direction sensitivity graphs of average bias and RMSE for each hour of the day. Figure (a) shows the the results for the GLOBE dataset, demonstrating the average bias (a1) and average RMSE (a2) for each wind direction bin. Similarly, (b1) and (b2) demonstrate the average bias and RMSE, respectively, for the FLOW dataset. The three colors indicate the three different lidar ABLH averaging techniques.)

The ToD average was calculated to provide a realistic characterization of the boundary layer, where the mixing layer defines the daytime, convective conditions and the residual layer defines the nighttime, stable atmosphere. The mix of both boundary

https://doi.org/10.5194/wes-2025-155
Preprint. Discussion started: 20 October 2025

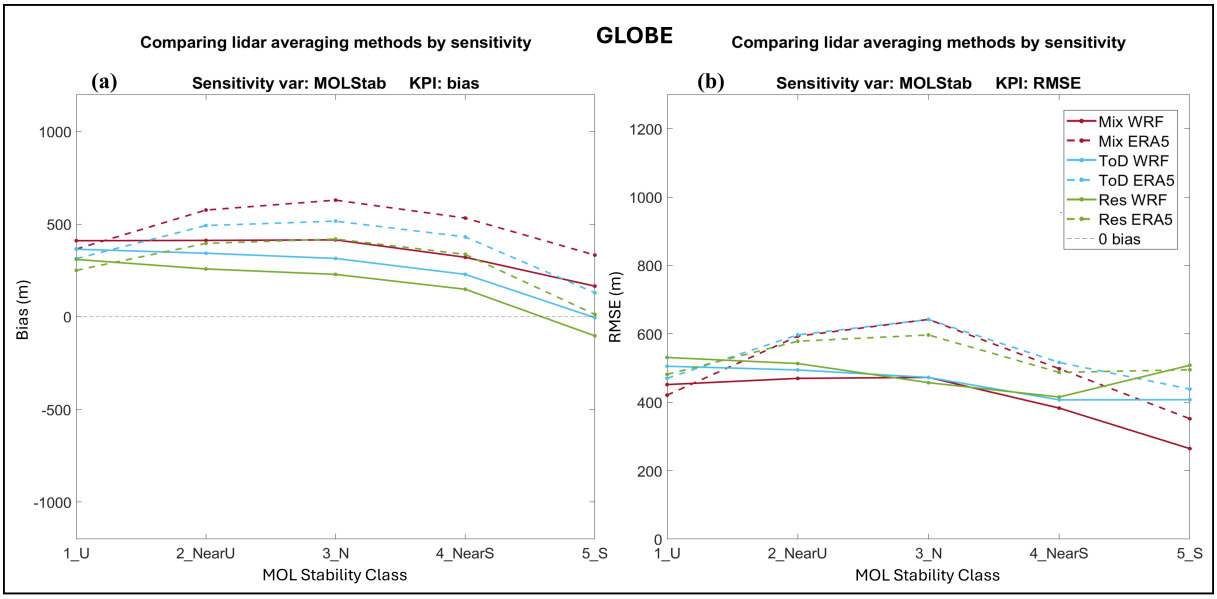

Figure 17. Stability classification sensitivity graphs based on the MOL for only the GLOBE dataset. The x axis denotes the five stability condition bins and the y axis the bias (a) and RMSE (b)

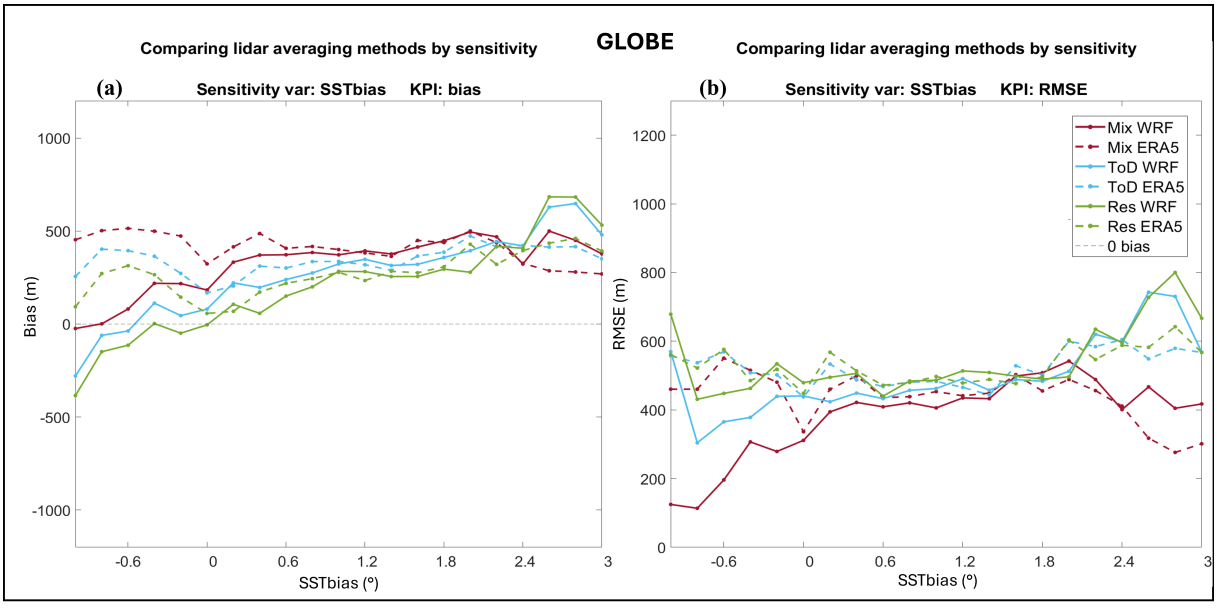

Figure 18. SST bias from measurement to model sensitivity graphs for the GLOBE dataset. The x axis denotes the SST bias bins and the y axis the bias (a) and RMSE (b)

https://doi.org/10.5194/wes-2025-155
Preprint. Discussion started: 20 October 2025

eawe european academy of wind energy
Open Access WIND ENERGY SCIENCE DISCUSSIONS

layer definitions in the analysis yields an artificial bias in the diurnal cycle sensitivity, as the residual layer tends to yield greater biases and RMSE than the mixing layer average.

The choice between mixing or residual layer height as the true ABLH depends on the application. The boundary layer height evolves with diurnal turbulence regimes; wind turbine wakes add to this momentum flux and increase entrainment. At night, however, the turbulence dissipates and the ABL can only be defined by the passage of aerosols. This is why the ToD average provides accurate ABL insight as it considers the ABL definitions during the appropriate conditions.

The results do not demonstrate a clear advantage or disadvantage between WRF and ERA5. Based on the RMSE results, both models show similar difference from the lidar measurements. The GLOBE dataset yields a greater overestimation from ERA5 than WRF, but the FLOW dataset demonstrates a lower bias from the ERA5 dataset than WRF.

The slightly closer correlation of WRF to the ABL measurements could be due to the integration of an ABL scheme, rather than the calculation of a critical Richardson number as in ERA5. The boundary layer scheme used in WRF for this analysis was MYNN, and is based on an eddy diffusivity component which calculates the TKE budget, mixing lengths, and stability functions to obtain the boundary layer height (Olson et al., 2019). The inclusion of the TKE budget also accounts for buoyancy production via the Brunt-Vaisala frequency, which also includes an entrainment efficiency term. This term, however, is a product of a constant that may not be well tuned for stable conditions. Additionally, unlike ERA5 which depends on a critical Richardson number, the MYNN stability functions are formulated to allow small finite momentum mixing to exist as the Richardson number approaches infinity. In Olson et al. (2019), however, they note that this requires adjusting other closure constants that results in increased mixing in stable conditions, thus potentially increasing the boundary layer height indirectly.

The main sensitivities that were found were related to the diurnal cycle, SST bias of model and on-site measurement, and a slight sensitivity to wind direction. The stability characterization of the MOL did not show any correlation with the bias. The lack of data in neutral conditions leads to an insufficient determination on this sensitivity. Both sites and a majority comparisons made with three lidar ABL averaging techniques demonstrated higher biases during the night, and lower during the day. As previously noted, the models seem to have better correlation with the lidar mixing layer retrieval potentially due to the their turbulence-defined ABL schema definition of the ABL. During nighttime conditions are more stable, and mesoscale models are known to be less accurate during these conditions (Olson et al., 2019) (Cañadillas et al., 2022). The SST bias of the models and measurement appears to have the greatest sensitivity, indicating misrepresentation of heat flux parameterizations could be the cause of the ABL over and underestimations. The slight directional sensitivity in the GLOBE dataset could be due to wind farm wakes from certain wind directions; the wind farm is not parameterized in the models, thus skewing the results.

The results of the analysis highlight the importance of the ABLH definition in all stability conditions, as well as the lack of consistency between ABLH mesoscale model outputs and lidar measurement. The dual representation of the boundary layer in stable and turbulent conditions greatly impacts the comparison with mesoscale models. The ABLH is a function of both convective activity and aerosol concentration, thus both atmospheric components should be accurately modeled in order to understand impacts of momentum flux on this energy entrainment.

The inconsistency of results between the GLOBE and FLOW datasets could be attributed to the difference in site characteristics. The FLOW site is coastal and the subgrid, unstable conditions of the site are not well parameterized leading to an

https://doi.org/10.5194/wes-2025-155
Preprint. Discussion started: 20 October 2025

underestimation of the ABLH. The residual layer retrievals from the FLOW site yielded high ABLHs, leading to an underesti-
400 mation from the models. The greatest errors came from land-based winds, so it is possible that certain atmospheric phenomena such as dust events or low level jets result in higher backscatter profiles. This leads to higher ABLHs from the lidar residual layer retrieval compared to the models. It is also possible the grid location from WRF and ERA5 did not accurately capture the coastal atmospheric conditions within the parameterizations for boundary layer conditions. The comparative analysis between both sites shows a more consistent bias and error with the lidar measurements in completely offshore conditions for the
405 GLOBE campaign and more variable results for the coastal location of the FLOW campaign.

The RMSE is quite high in all circumstances, ranging from around 300m to almost 800m difference from model to measurement. This is significant enough to create uncertainty in both WRF and ERA5 validity in ABL representation, and highlights the need for further validation. Scanning lidar ABLH measurements represent a credible reference for boundary layer height conditions. The lidar measurements used to derive the ABLH are already trusted to give accurate depictions of wake characteristics from both radial wind speeds and CNR, as well as reconstructed wind speeds for wind resource assessment. Therefore the significant difference between the lidar and model ABLHs can be confidently attributed to model misrepresentation rather than miscalculation from the lidar derivation. Mesoscale model ABL characterization is based on physical equations defining stability regimes such as turbulence and heat flux, which do not always accurately capture ABLH conditions. The mixing and residual layer definitions from the lidar can help correct the model parameterizations to conditions where the ABL scheme is
415 not well tuned, especially for the residual layer representing more stable conditions. The models yielded closer results to the mixing layer height derived from the lidar, yet the residual layer derivation still represents a valid characterization of the ABL as it is based on the intensity of aerosols in the atmosphere.

5 Conclusion

With the projected increased investment in offshore wind, it is important to accurately model atmospheric conditions to under-
420 stand wake impacts and wind farm power performance. Previous studies demonstrate the significance of the ABLH to impact wake augmentation and dissipation rates by affecting the entrainment area for the momentum flux of the wake to dissipate. This research aims to fill the gap of model ABLH validation by comparing to lidar ABLH retrievals in offshore conditions. Two scanning lidar campaigns were compared with WRF and ERA5 ABLH outputs for bias and RMSE comparisons. The lidar ABLH retrievals provided altitudes for the mixing and residual layer, so three different averages were compared with the
425 model ABLH outputs: an average of only mixing layer altitudes, an average of only residual layer altitudes, and an average based on the time of day where only residual layer heights were averaged at night, and mixing layer heights during the day.

The results showed a wide disparity between the measurements and the models. Both ERA5 and WRF found greater correlation with the lidar ABLH mixing layer retrievals, indicating the basis of ABL characterization of mesoscale models using turbulence-based derivations. WRF performed more accurately for the GLOBE dataset, while ERA5 yielded slightly more
430 accurate results for the FLOW dataset. The sensitivity analysis exposed a significant correlation with ABLH bias of the models and measurement to SST biases, indicating that a misrepresentation of surface heat fluxes could impact the ABLH derivation

https://doi.org/10.5194/wes-2025-155
Preprint. Discussion started: 20 October 2025

methods for both ERA5, which is based on the critical Richardson number, and WRF, based on an eddy-diffusivity boundary layer scheme. The results from both campaigns did not yield a clear and consistent bias of the models with the measurements, demonstrating a simple bias correction is not possible. Additional research must be conducted to pinpoint the sensitivity of this bias in various stability conditions.

Further investigation should include assessing various stability parameterizations to better represent ABL characteristics. Lidar ABLH retrievals vary depending on mixing or residual layer definition, so further studies should be conducted to understand the boundary layer definition based on remote sensing techniques to define when backscatter or vertical velocity gradients provide accurate representation of the marine boundary layer. Additionally, this study could further improve the validity of lidar boundary layer height retrievals by comparing different methods to derive the height including image processing, various gradient processing techniques, and inclusion of machine learning methods. The absence of an absolute reference for the ABLH, as well as multiple physical definitions on how to derive it, leads to the uncertainty investigated in this study. The wind energy industry would benefit from a consolidation and comparison of ABLH retrievals in all stability conditions to validate wake modeling ABL characterization and ensure accurate power production representation.

Author contributions. All authors have accepted responsibility for the entire content of this manuscript and consented to its submission to the journal, reviewed all the results and approved the final version of the manuscript.

Competing interests. At least one of the co-authors is a member of the editorial board of Wind Energy Science.

Acknowledgements. The GLOBE data used for this study was collected as part of the X-Wakes project funded by the Ministry for Economic Affairs and Climate Action (BMWK) under grant number FKZ 03EE3008A from the German Bundestag. The FLOW dataset comes from the FLOW project, a Horizon Europe funded project.

This research is conducted as part of the APTWind project funded by the Marie Sklodowska-Curie Actions under grand number 101119550. Thanks to the previous work on the GLOBE dataset from Lin-Ya Hung and Pedro Santos this research could take its next steps. Thanks to Bjarke Olsen and Martin Dorenkamper for providing the WRF datasets for both the FLOW and WRF simulations.

https://doi.org/10.5194/wes-2025-155
Preprint. Discussion started: 20 October 2025

eawe european academy of wind energy
Open Access WIND ENERGY SCIENCE DISCUSSIONS

References

Abraham, A., Puccioni, M., Jordan, A., Maric, E., Bodini, N., Hamilton, N., Letizia, S., Klein, P. M., Smith, E., Wharton, S., Gero, J., Jacob, J. D., Krishnamurthy, R., Newsom, R. K., Pekour, M., and Moriarty, P.: Operational wind plants increase planetary boundary layer height: An observational study, https://doi.org/10.5194/wes-2024-148, 2024.

Adams, N., Rodaway, C., Gottschall, J., Hawkes, G., and Simon, E.: WESC 2023 Mini-Symposium - OWA GloBE: Building Industry Consensus on the Global Blockage Effect in Offshore Wind, https://doi.org/10.5281/ZENODO.8085205, publisher: Zenodo, 2023.

Bianco, L. and Wilczak, J. M.: Convective Boundary Layer Depth: Improved Measurement by Doppler Radar Wind Profiler Using Fuzzy Logic Methods, Journal of Atmospheric and Oceanic Technology, 19, 1745–1758, https://doi.org/10.1175/1520-0426(2002)019<1745:CBLDIM>2.0.CO;2, 2002.

Bianco, L., Wilczak, J. M., and White, A. B.: Convective Boundary Layer Depth Estimation from Wind Profilers: Statistical Comparison between an Automated Algorithm and Expert Estimations, Journal of Atmospheric and Oceanic Technology, 25, 1397–1413, https://doi.org/10.1175/2008JTECHA981.1, 2008.

Cañadillas, B., Beckenbauer, M., Trujillo, J. J., Dörenkämper, M., Foreman, R., Neumann, T., and Lampert, A.: Offshore wind farm cluster wakes as observed by long-range-scanning wind lidar measurements and mesoscale modeling, Wind Energy Science, 7, 1241–1262, https://doi.org/10.5194/wes-7-1241-2022, 2022.

Dörenkämper, M., Witha, B., Steinfeld, G., Heinemann, D., and Kühn, M.: The impact of stable atmospheric boundary layers on wind-turbine wakes within offshore wind farms, Journal of Wind Engineering and Industrial Aerodynamics, 144, 146–153, https://doi.org/https://doi.org/10.1016/j.jweia.2014.12.011, selected papers from the 6th International Symposium on Computational Wind Engineering CWE 2014, 2015.

Eliassen, L., Jakobsen, J. B., and Obhrai, C.: ISOPE-2012 Rhodes: conference proceedings ; the proceedings of the Twenty-Second (2012) International Offshore and Polar Engineering Conference ; Rhodes, Greece, June 17 - 22, 2012 ; [including 7 specialty symposia], International Society of Offshore and Polar Engineers (ISOPE), Cupertino, Calif, ISBN 978-1-880653-94-4, 2012.

Fitch, A. C., Olson, J. B., Lundquist, J. K., Dudhia, J., Gupta, A. K., Michalakes, J., and Barstad, I.: Local and Mesoscale Impacts of Wind Farms as Parameterized in a Mesoscale NWP Model, Monthly Weather Review, 140, 3017–3038, https://doi.org/10.1175/MWR-D-11-00352.1, 2012.

Flamant, C., Pelon, J., Flamant, P. H., and Durand, P.: LIDAR DETERMINATION OF THE ENTRAINMENT ZONE THICKNESS AT THE TOP OF THE UNSTABLE MARINE ATMOSPHERIC BOUNDARY LAYER, Boundary-Layer Meteorology, 83, 247–284, https://doi.org/10.1023/A:1000258318944, 1997.

Guo, J., Zhang, J., Shao, J., Chen, T., Bai, K., Sun, Y., Li, N., Wu, J., Li, R., Li, J., Guo, Q., Cohen, J. B., Zhai, P., Xu, X., and Hu, F.: A merged continental planetary boundary layer height dataset based on high-resolution radiosonde measurements, ERA5 reanalysis, and GLDAS, Earth System Science Data, 16, 1–14, https://doi.org/10.5194/essd-16-1-2024, 2024.

Hersbach, H., Bell, B., Berrisford, P., Hirahara, S., Horányi, A., Muñoz-Sabater, J., Nicolas, J., Peubey, C., Radu, R., Schepers, D., Simmons, A., Soci, C., Abdalla, S., Abellan, X., Balsamo, G., Bechtold, P., Biavati, G., Bidlot, J., Bonavita, M., De Chiara, G., Dahlgren, P., Dee, D., Diamantakis, M., Dragani, R., Flemming, J., Forbes, R., Fuentes, M., Geer, A., Haimberger, L., Healy, S., Hogan, R. J., Hólm, E., Janisková, M., Keeley, S., Laloyaux, P., Lopez, P., Lupu, C., Radnoti, G., de Rosnay, P., Rozum, I., Vamborg, F., Villaume, S., and Thépaut, J.-N.: The ERA5 global reanalysis, Quarterly Journal of the Royal Meteorological Society, 146, 1999–2049, https://doi.org/https://doi.org/10.1002/qj.3803, 2020.

https://doi.org/10.5194/wes-2025-155
Preprint. Discussion started: 20 October 2025

Hu, X.-M., Nielsen-Gammon, J. W., and Zhang, F.: Evaluation of Three Planetary Boundary Layer Schemes in the WRF Model, Journal of Applied Meteorology and Climatology, 49, 1831 – 1844, https://doi.org/10.1175/2010JAMC2432.1, 2010.

Jozef, G., Cassano, J., Dahlke, S., and De Boer, G.: Testing the efficacy of atmospheric boundary layer height detection algorithms using uncrewed aircraft system data from MOSAiC, Atmospheric Measurement Techniques, 15, 4001–4022, https://doi.org/10.5194/amt-15-4001-2022, 2022.

Kalvig, S., Gudmestad, O. T., and Winther, N.: Exploring the gap between 'best knowledge' and 'best practice' in boundary layer meteorology for offshore wind energy, Wind Energy, 17, 161–171, https://doi.org/10.1002/we.1572, 2014.

Krishnamurthy, R., Newsom, R. K., Kaul, C. M., Letizia, S., Pekour, M., Hamilton, N., Chand, D., Flynn, D., Bodini, N., and Moriarty, P.: Observations of wind farm wake recovery at an operating wind farm, Wind Energy Science, 10, 361–380, https://doi.org/10.5194/wes-10-361-2025, 2025.

Li, X., Dong, Y., Zhang, Y., Shi, Z., and Yao, J.: Climatology of Planetary Boundary Layer Height over Jiangsu, China, Based on ERA5 Reanalysis Data, Atmosphere, 14, https://doi.org/10.3390/atmos14091330, 2023.

Liu, S. and Liang, X.-Z.: Observed Diurnal Cycle Climatology of Planetary Boundary Layer Height, Journal of Climate, 23, 5790–5809, https://doi.org/10.1175/2010JCLI3552.1, 2010.

Lundquist, J. K., Takle, E. S., Boquet, M., Kosović, B., Rajewski, D., Doorenbos, R., Irvin, S., Aitken, M. L., Quelet, P. T., Rana, J., Martin, C. S., and Vanderwende, B.: Lidar observations of interacting wind turbine wakes in an onshore wind farm, https://www.nrgsystems.com/assets/resources/Lidar-observations-of-interacting-wind-turbine-wakes-Whitepaper.pdf, 2014.

Moreira, G. D. A., Guerrero-Rascado, J. L., Bravo-Aranda, J. A., Foyo-Moreno, I., Cazorla, A., Alados, I., Lyamani, H., Landulfo, E., and Alados-Arboledas, L.: Study of the planetary boundary layer height in an urban environment using a combination of microwave radiometer and ceilometer, Atmospheric Research, 240, 104 932, https://doi.org/https://doi.org/10.1016/j.atmosres.2020.104932, 2020.

Munters, W. and Meyers, J.: An optimal control framework for dynamic induction control of wind farms and their interaction with the atmospheric boundary layer, Philosophical Transactions of the Royal Society A: Mathematical, Physical and Engineering Sciences, 375, 20160 100, https://doi.org/10.1098/rsta.2016.0100, 2017.

Olsen, B. T. E., Hahmann, A. N., Alonso-de Linaje, N. G., Žagar, M., and Dörenkämper, M.: Low-level jets in the North and Baltic Seas: Mesoscale Model Sensitivity and Climatology, https://doi.org/10.5194/egusphere-2024-3123, 2024.

Olson, J. B., Kenyon, J. S., Angevine, W. A., Brown, J. M., Pagowski, M., and Sušelj, K.: A Description of the MYNN-EDMF Scheme and the Coupling to Other Components in WRF–ARW, https://doi.org/10.25923/N9WM-BE49, publisher: Earth System Research Laboratory (U.S.), Global Systems Division, 2019.

Optis, M., Monahan, A., and Bosveld, F.: Moving Beyond Monin–Obukhov Similarity Theory in Modelling Wind-Speed Profiles in the Lower Atmospheric Boundary Layer under Stable Stratification, Boundary-Layer Meteorology, 153, 497–514, https://doi.org/10.1007/s10546-014-9953-z, 2014.

Patel, A., Mann, J., Sjoholm, M., Thorsen, G., Simon, E., Syed, A., Hung, L., and Gottschall, J.: Lidar observations of turbulence for tall offshore 2 wind turbines, 2025.

Puccioni, M., Moss, C. F., Solari, M. S., Roy, S., Iungo, G. V., Wharton, S., and Moriarty, P.: Quantification and assessment of the atmospheric boundary layer height measured during the AWAKEN experiment by a scanning LiDAR, Journal of Renewable and Sustainable Energy, 16, 053 304, https://doi.org/10.1063/5.0211259, 2024.

https://doi.org/10.5194/wes-2025-155
Preprint. Discussion started: 20 October 2025

Sandu, I., Beljaars, A., Bechtold, P., Mauritsen, T., and Balsamo, G.: Why is it so difficult to represent stably stratified conditions in numerical weather prediction (NWP) models?, Journal of Advances in Modeling Earth Systems, 5, 117–133, https://doi.org/10.1002/jame.20013, 2013.

Sathe, A. and Bierbooms, W.: Influence of different wind profiles due to varying atmospheric stability on the fatigue life of wind turbines, Journal of Physics: Conference Series, 75, 012 056, https://doi.org/10.1088/1742-6596/75/1/012056, 2007.

Schneemann, J., Theuer, F., Rott, A., Dörenkämper, M., and Kühn, M.: Offshore wind farm global blockage measured with scanning lidar, Wind Energy Science, 6, 521–538, https://doi.org/10.5194/wes-6-521-2021, publisher: Copernicus GmbH, 2021.

Seidel, D. J., Zhang, Y., Beljaars, A., Golaz, J.-C., Jacobson, A. R., and Medeiros, B.: Climatology of the planetary boundary layer over the continental United States and Europe, Journal of Geophysical Research: Atmospheres, 117, https://doi.org/https://doi.org/10.1029/2012JD018143, 2012.

Shen, Z., Liu, L., Lu, X., and Stevens, R. J.: The global properties of nocturnal stable atmospheric boundary layers, Journal of Fluid Mechanics, 999, A60, https://doi.org/10.1017/jfm.2024.969, 2024.

Sood, I., Munters, W., and Meyers, J.: Effect of conventionally neutral boundary layer height on turbine performance and wake mixing in offshore windfarms, Journal of Physics: Conference Series, 1618, 062 049, https://doi.org/10.1088/1742-6596/1618/6/062049, 2020.

Stull, R.: An Introduction to Boundary Layer Meteorology, Kluwer Academic Publishers, 1988.

Veers, P., Dykes, K., Basu, S., Bianchini, A., Clifton, A., Green, P., Holttinen, H., Kitzing, L., Kosovic, B., Lundquist, J. K., Meyers, J., O'Malley, M., Shaw, W. J., and Straw, B.: Grand Challenges: wind energy research needs for a global energy transition, Wind Energy Science, 7, 2491–2496, https://doi.org/10.5194/wes-7-2491-2022, 2022.

Vogelezang, D. and Holtslag, B.: Evaluation and model impacts of alternative boundary-layer height formulations, Boundary-Layer Meteorology, 81, 245–269, https://doi.org/10.1007/BF02430331, 1996.

Xi, X., Yang, Q., Liu, C., Shupe, M. D., Han, B., Peng, S., Zhou, S., and Chen, D.: Evaluation of the Planetary Boundary Layer Height From ERA5 Reanalysis With MOSAiC Observations Over the Arctic Ocean, Journal of Geophysical Research: Atmospheres, 129, e2024JD040 779, https://doi.org/10.1029/2024JD040779, 2024.

Xu, S., Zhuang, T., Zhao, W., and Wan, D.: Numerical investigation of aerodynamic responses and wake characteristics of a floating offshore wind turbine under atmospheric boundary layer inflows, Ocean Engineering, 279, 114 527, https://doi.org/10.1016/j.oceaneng.2023.114527, 2023.